Beatriz Condeço Pinto Pagará

Licenciatura em Ciências de Engenharia de Micro e Nanotecnologias

Paper as a Colorimetric Biosensing Platform for Tetracyclines Detection in Milk

Dissertação para obtenção do Grau de Mestre em Engenharia de Micro e Nanotecnologias

Orientador: Elvira Maria Correia Fortunato, Prof. Doutora, FCT-UNL

Júri:

Presidente: Prof. Doutor Hugo Manuel Brito Águas
Arguente: Prof. Doutor Pedro Fernandes Antunes
Vogal: Prof. Doutora Elvira Maria Correia Fortunato

FACULDADE DE CIÊNCIAS E TECNOLOGIA
UNIVERSIDADE NOVA DE LISBOA

Outubro 2018

Paper as a Colorimetric Biosensing Platform for Tetracyclines Detection in Milk

Dedicado aos meus pais.

Acknowledgment

Chegou ao fim uma etapa bastante importante na minha vida. O que parecia tão distante há cinco anos atrás, está agora a chegar ao fim, dando abertura a novas oportunidades e a novos conhecimentos. Foram anos que me fizeram crescer, e que acima de tudo me deram uma outra perspetiva da vida e dos outros. Durante estes anos fui acompanhada por pessoas bastante importantes sem as quais não seria possível ter chegado onde cheguei.

Antes de mais gostaria de agradecer à minha instituição de ensino, a Faculdade de Ciências e Tecnologia da Universidade Nova de Lisboa e ao Departamento de Ciências dos Materiais, por me terem integrado da melhor forma e por me permitirem desenvolver os meus conhecimentos.

Gostaria também de agradecer à minha orientadora, Professora Elvira Fortunato pela transmissão de conhecimentos e por todo o acompanhamento ao longo deste trabalho.

Um especial agradecimento à Carolina Marques pela disponibilidade que sempre teve em ajudar-me e por toda a paciência que demonstrou de forma a esclarecer sempre as minhas dúvidas. Obrigada por toda a ajuda incansável, pela motivação e pela confiança que sempre me transmitiu.

Ao João Ferrão pela ajuda sempre disponível e por todas as opiniões e críticas que também contribuíram para a realização deste trabalho.

A toda a equipa do CENIMAT, pelo bom ambiente, boa disposição e espírito de entreajuda. Aos meus colegas de laboratório, pela companhia das longas horas no laboratório, pelas conversas e bom ambiente.

Aos grandes amigos que criei nestes cinco anos de faculdade, foi um prazer ter-vos conhecido. Sem vocês, não seria a mesma coisa. Obrigada pelos jantares, festas, pelos serões de estudo e de desespero. Fizeram com que valesse a pena. Espero que a vida nos continue a proporcionar mais momentos juntos e que a nossa amizade perdure.

Às minhas amigas de longa data, que apesar de longe estão sempre presentes. Obrigada por todo o apoio e amizade. Sei que são amizades que tenho para a vida.

Ao Cristóvão, obrigada por me aturares estes anos todos. Obrigada pelo apoio, amor e sobretudo pela amizade.

Obrigada à minha família e em especial aos meus pais. São a minha maior motivação e o meu maior exemplo. Sem vocês sem dúvida que não teria conseguido chegar onde cheguei. Vocês são a razão disto tudo. Obrigada pelo apoio incondicional, pelo amor e educação. Estarei em dívida para convosco por todo o esforço que realizaram por forma a permitir a minha integração, o meu crescimento e a minha continuação nos estudos. Obrigada por sempre acreditarem em mim. Espero que se sintam orgulhosos.

Por fim, um agradecimento muito especial às minhas avós que sempre sonharam em presencear este momento, mas que infelizmente não conseguiram realizar esse sonho. Espero que estejam a olhar por mim.

Abstract

Tetracyclines are a type of antibiotic that exhibits activity against most gram-positive and gram-negative bacteria. These antibiotics are often added at subtherapeutic levels to feed to act as growth promoters. Due to its low bioavailability, only a fraction of the antibiotic is metabolized in animals, causing waste. These residues can enter human bodies through the food chain and lead to increased antimicrobial resistance, causing allergic or toxic reactions, which led several countries to implement a maximum level of residues for this type of antibiotic. Most methods of detecting TCs are time consuming or inadequate for field analysis. In this way, an inexpensive, easy-to-execute and fast analytical method is required.

In this sense, in the present work a colorimetric biosensor was developed in paper for the detection of four type of tetracyclines, presenting an alternative in the performance of point-of-care tests. Paper is low-cost, abundant, biodegradable and easy to dispose of by incineration.

The construction of the sensors was performed using Lab-on-Paper technology and is based on the synthesis of gold nanoparticles by reducing a gold salt in which tetracyclines constitute the reducing agent itself. Different concentrations of TCs result in the formation of different colour intensities.

Different concentrations of tetracyclines were tested and analysed using *ImageJ* software, allowing linear calibration lines to be obtained, that relate the concentration of antibiotics in a range between 0.1 and 10 µg/mL and the arithmetic mean of the RGB channels.

Validation tests of the sensors developed with TC in milk were also performed. It was observed that it is possible to detect this type of antibiotic in pre-treated milk, and four forms of milk treatment were studied.

KEYWORDS: Tetracycline antibiotics; colorimetric assay; gold nanoparticles; paper-based biosensors; milk.

Resumo

As tetraciclinas são um tipo de antibiótico que exibe atividade contra a maioria das bactérias gram-positivas e gram-negativas. Estes antibióticos são muitas vezes adicionados em níveis subterapêuticos aos alimentos para animais de modo a atuar como promotores de crescimento. Devido à sua baixa biodisponibilidade, apenas uma fração do antibiótico é metabolizada nos animais, causando resíduos. Esses resíduos podem entrar nos corpos humanos através da cadeia alimentar e levar ao aumento da resistência antimicrobiana, causando reações alérgicas ou tóxicas, o que levou vários países a implementarem um nível máximo de resíduos para este tipo de antibiótico. A maioria dos métodos de deteção de TCs é demorada ou inadequada para análise de campo. Desta forma, é solicitado um método analítico barato, fácil de executar e rápido.

Neste sentido, no presente trabalho desenvolveu-se um biossensor colorimétrico em papel para a deteção de quatro tipo de tetraciclinas, apresentando uma alternativa na realização de testes *point-of-care*. O papel é de baixo custo, existe em abundância, é biodegradável e é de fácil eliminação por incineração.

A construção dos sensores foi efetuada recorrendo à tecnologia *Lab-on-Paper* e baseia-se na síntese de nanopartículas de ouro por redução de um sal de ouro em que as tetraciclinas constituem o próprio agente redutor. Diferentes concentrações de TCs resultam na formação de diferentes intensidades de cor.

Foram testadas e analisadas diferentes concentrações de tetraciclinas através do *software ImageJ*, permitindo obter as retas de calibração lineares que relacionam a concentração dos antibióticos num intervalo entre 0.1 e 10 µg/mL, e a média aritmética dos canais RGB.

Testes de validação dos sensores desenvolvidos com TC em leite foram realizados. Observou-se que é possível detetar este tipo de antibiótico no leite pré-tratado, e quatro formas de tratamento do leite foram estudadas.

PALAVRAS-CHAVE: Tetraciclinas; ensaio colorimétrico; nanopartículas de ouro; biossensores baseados em papel; leite.

Abbreviations

a.u. – Arbitrary Units
AuNPs – Gold nanoparticles
CTAC – Cetyltrimethylammonium chloride
CENIMAT – *Centro de Investigação de Materiais*
CTC – Chlortetracycline
CV – Coefficient of Variation
DC – Doxycycline
EDS – Energy Dispersive X-ray Spectroscopy
ELISA – Enzyme-linked Immunosorbent Assays
FPT – Four Plate Test
FTIR – Fourier-Transform Infrared Spectroscopy
LOD – Limit of Detection
LOQ – Limit of Quantitation
MRL – Maximum Residual Level
OTC – Oxytetracycline
RGB – Red Green Blue
SD – Standard Deviation
SEM – Scanning Electron Microscopy
SPFIA – Solid-phase Fluorescence Immunoassays
SPR – Surface Plasmon Ressonance
TC – Tetracycline
TCs – Groupe of tetracyclines antibiotics
UV-Vis – Visible and Ultraviolet radiation
XRD – X-ray Diffraction
µPADs – Microfluidic Paper-based Analysis Devices

Symbols

Au – Gold

AuCl$_4^-$ - Tetrachlorogold (1-)

C – Carbon

CaCO$_3$ – Calcium carbonate

CH$_2$ – Methylene

Cl – Chloride

$CH_3(CH_2)_{15}N(Cl)(CH_3)_3)$ – Cetyltrimethylammonium chloride

$C_{22}H_{24}N_2O_8$•**HCl** – Tetracycline hydrochloride

$C_{22}H_{24}N_2O_8$•**HCl•0,5H$_2$O•0,5C$_2$H$_6$O** – Doxycycline hyclate

$C_{22}H_{24}N_2O_9$•**HCl** – Oxytetracycline hydrochloride

$C_{22}H_{23}ClN_2O_8$•**HCl** – Chlortetracycline hydrochloride

H – Hydrogen

H$^+$ - Hydrogen (1+)

HAuCl$_4$ – Chloroauric acid tetrahydrate

HAuCl_4•3H_2O – Tetrachloroaurate tri-hydrate

Na – Sodium

$Na_2B_4O_7$ – Sodium tetraborate buffer

O – Oxygen

OH – Hydroxide

g – Grams

mg – Milligrams

mL – Millilitres

kg – Kilograms

µm – Micrometer

µL – Microliter

µg – Microgram

cm^2 – Centimeter squared

cm^{-1} – Centimeter high to minus 1

m^2 – Square meter

m^3 – Cubic meter

mM – Millimolar

M – Molar

keV – Kilo electron-volt

º - Angle

ºC – Degrees Celsius

% - Percentage

θ - Bragg Angle

ρ$_{fiber}$ – Fiber density

ρ$_{paper}$ – Paper density

I$_{AM}$ – Intensity for amorphous material

I$_{200}$ – Intensity for 200 peak

b – Slope

S$_a$ – Standard deviation

x_{CR} – Sample crystallinity

Table of Contents

List of Figures

List of Tables

Motivation and Objectives

Tetracyclines are low cost and broad-spectrum antibiotics commonly used for the prevention and treatment of dairy cattle for several bacterial infections or as additives to promote growth in farm animals. The extensive use of this type of antibiotics in veterinary medicine has led to their accumulation in diary food products, such as milk.

In this way, their monitoring is very important in controlling the safety of milk for human consumption because the presence of these drug residues can trigger potential adverse side effects in humans such as allergic reactions in hypersensitive individuals and other long-term health effects, or they can be potential carcinogenic. In fact, at present, up to 10% of people have already been diagnosed to be hypersensitive or allergic to antibiotics.

Strict legislative regulations have been imposed for the treatment of animals with antibiotics and maximum residue limits (MRLs) in foods of animal origin, established for residues of antibiotics or their metabolites. Thus, to ensure food safety and protect the health of consumers, there have been lots of efforts to develop various strategies for the detection and quantification of tetracycline in food products. However, most methods of detecting this type of antibiotic are complex, expensive, time consuming or not suitable for field analysis.

Paper has emerged in recent years as a suitable material to be used as support in biological and chemical tests offering several advantages such as low cost, easy handling, disposability, biocompatibility, biodegradability and even ease of disposal by incineration.

In this sense, the main purpose of this dissertation is to enhance the properties and advantages offered by paper through Lab-on-Paper technology, developing a colorimetric biosensor to determine the concentration of four types of tetracyclines in milk.

The main steps of this work included:

i. Analysis and characterization of two different types of paper from the structural, chemical and morphological point of view;
ii. Synthesis and characterization of gold nanoparticles obtained by reduction with the tetracyclines under study, in order to obtain a colorimetric detection of the same;
iii. Use of Lab-on-Paper technology in the production of paper sensors for subsequent application to determine the concentration of tetracyclines;
iv. Calibration of the sensors through digital analysis, using aqueous solutions with different tetracyclines concentrations;
v. Optimization of the sensor for the detection of tetracyclines in milk samples.

Therefore, this works aims to obtain an innovative, simple and inexpensive method for the detection of tetracyclines in milk samples, thus contributing to the control and reduction of potential adverse side effects in human's health.

<div align="right">

Chapter 1
Introduction

</div>

1.1 Paper

Paper consists predominantly of a network of cellulose fibers, a polymer composed of glucose monomers bound linearly and covalently by β-1,4-glycosidic bonds. This network is chemically bonded by hydrogen bonds and is organized in the form of microfibrils, forming the crystalline unit of cellulose. Cellulose is one of the main constituents of plant cell walls. Two other major components of plant cell walls are hemicellulose and lignin. Hemicellulose is composed of pentoses and monomers, and forms a strong matrix surrounding the cellulose fibers from hydrogen and *Van der Waals* bonds. Lignin has a complex and photosensitive structure and is therefore normally removed during the papermaking process. [1], [2]

The material most used as a source of cellulose is the wood of trees, due to its low cost and easy to obtain. Cellulose fibers can also be extracted from bamboo, jute, hemp, flax, cotton and some grasses (wheat, barley or rice). [3]

The manufacture of a paper sheet involves several steps which are summarized in **Figure 1.1**. It should be noted that prior to the production of paper the reduction of the raw material to a fibrous pulp is necessary. The processes of formation of this paste are called pulping processes and can be divided into two types: chemical (removal of the lignin from chemical agents, heat and pressure) or mechanical (grinding of the wood). [2], [3]
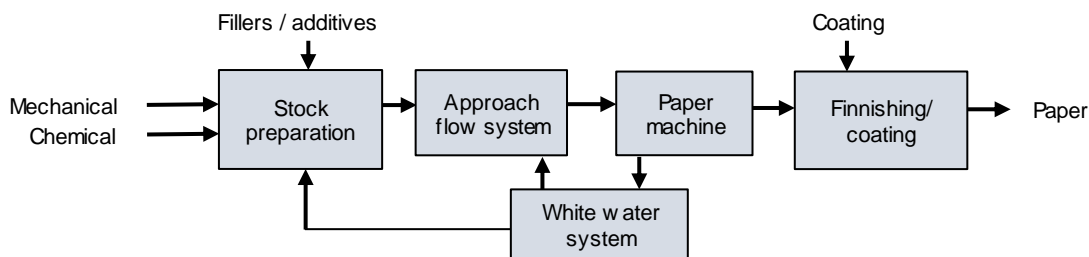
Figure 1.1- Schematic of paper manufacturing.

1.2 Biosensors

A biosensor is an instrument that always depends on a transducer and a recognition element with a carrier material. The transducer can detect any interaction between two elements whose affinity is high (antibodies/antigens, enzymes/substrates, receptors and ligands or living cells and analyte that specifically binds to them). This interaction is converted into a measurable signal for interpretation by the processor, which then converts it into a measurable output. [4], [5]

They are mainly used for control in the clinical and environmental areas, with the main objective being the development of rapid diagnostic tests for point-of-care. [6]

1.2.1 Paper-based biosensors

Paper can be hydrophilic and porous, thus providing a natural platform for fabricating microfluidic channels for multiplex analyte detection, making it a good alternative to conventional microfluidics. [7], [8]

The paper biosensors can be divided into 3 categories: **Lateral flow assay**, that is performed over a strip divided in four different parts (sample application pad, conjugate pad, nitrocellulose membrane that is divided into test and control lines, and adsorption pad). The deposited sample moves easily through capillary forces of the material through a lateral flow in a predefined path in the porous membrane; [9], [10] **Dipstick paper**, based on immersion in the sample of a strip of paper with pre-deposited reagents; [6], [11], [12] **Microfluidic Paper**, based analysis devices which require a relatively lower sample volume compared to the previous devices. This type of paper biosensor, also called µPADs, can also be constructed in 3D format and usually use a type of colorimetric detection where results can be observed with the naked eye or with the aid of a mobile phone or a portable digitizer. [13], [14]

1.3 Lab-on-paper Technology

Lab-on-paper technology was introduced in 2007 by the need for a platform that uses small volumes of sample and that is sufficiently inexpensive to be widely used, making possible to run multiple diagnostic assays. [15], [16]

This technology can be described as a group of microchannel that provide spatial control of fluid sand and enable fluid transport by capillarity on hydrophilic paper. [15], [16] This microchannel can be created via patterning fabricated by various techniques like photolithography, inkjet printing, stamping, cutting, screen-printing and wax printing. Wax printing is the fastest and simplest fabrication. A solid ink printer and the solid wax is melted before being ejected from the print head, printing in this way the desired design. Then the printed paper is heated in a hot plate, allowing the wax to diffuse vertically through the porous paper. In this way, a hydrophobic barrier is created with the wax, enabling spatial control fluid transport. The device can be encapsulated preventing contamination, degradation and reducing fluid evaporation. [15], [17] The most commonly used paper as a support is chromatography paper Whatman, that has a lower cost comparing with nitrocellulose, used in lateral flow assays or microfluidics. [15]

1.4 Gold Nanoparticles

Gold nanoparticles (AuNPs) properties were probably first described by the year of 1600, when Parcelsus reported a red mixture formed by condensations of a gold colloid. Also Faraday, over 150 years ago, observed that colloidal gold solutions have properties that differ from bulk gold. [18]

Bulk gold has a familiar yellow colour, caused by a reduction in reflectivity for light at the end of the spectrum. But AuNPs, they are capable of absorbing green light at about 520 nm of the visible spectrum, appearing in ruby red. The physical origin of this phenomenon is associated with the coherent oscillation of AuNP surface electrons (localized surface plasmon) induced by the incident electromagnetic field. An absorption band results when the incident photon frequency is resonant with the collective oscillation of the conduction band electrons and is known as the surface plasmon resonance (SPR).

The resonance frequency of this SPR is strongly dependent upon the size, shape, interparticle interactions, dielectric properties, and local environment of the nanoparticle.

Also, the aggregation of AuNPs can change their colour from red to blue because of the shift of the surface plasmon band to longer wavelength, where the aggregate could be considered as a single large particle. [18], [19]
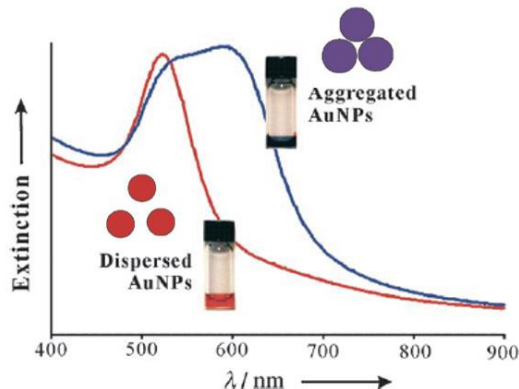
Figure 1.2- Surface plasmon absorption bands for AuNPs in the visible light region. The red and blue curves correspond to dispersed and aggregated AuNPs, respectively. Adapted from [19].

The use of noble metal nanoparticles (such as AuNPs) in biosensing has grown enormously in recent years, mainly due to detection that can often be carried out with the naked eye, yielding rapid, inexpensive and portable detection. [18], [20]

AuNPs features like particle size, shape, composition and surface coating can be manipulated for specific applications such as molecular recognition, chemical sensing and imaging. Furthermore, AuNPs have high surface-to-volume ratio and high surface energy to provide a stable immobilization of a large amount of biomolecules. [21]–[23]
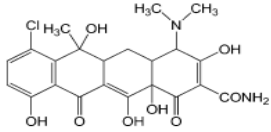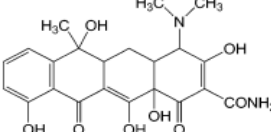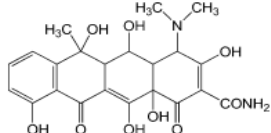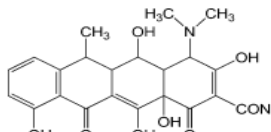
1.5 Tetracycline antibiotics

Tetracycline antibiotics (TCs) were discovered more than 50 years ago, and they have the capacity to prevent the attachment of aminoacyl-tRNA to the ribosomal acceptor (A) site, inhibiting protein synthesis. The first members of the tetracycline group to be described were chlortetracycline and oxytetracycline, discovered in 1940. [24], [25]

TCs are strong chelating agents and both their antimicrobial and pharmacokinetic properties are influenced by chelation of metal ions. TCs molecules contains a linear fused tetracyclic nucleus as a basic skeleton, to which a variety of functional groups are attached. These antibiotics only differ from each other chemically by substituent variations at carbons 5, 6 and 7. [24], [26] In **Table 1.1,** one can observe the chemical structures of four different tetracyclines.

This type of antibiotics has been widely used in human therapy and animal infections treatment due to their antimicrobial properties, exhibiting activity against most of gram-positive and gram-negative bacteria. Furthermore, in some countries, TCs are added at subtherapeutic levels to animal feeds to act as growth promoters. TCs have low bioavailability so only a fraction of the antibiotic is metabolized in the animals, causing residues. These residues can enter human bodies through the food chain and can lead to increased drug resistance of microbial strains in humans, causing allergic or toxic reactions and leads to a decrease in the efficacy of TCs in the treatment of various diseases. [24], [27]–[29]

Table 1.1- Structures of the tetracycline antibiotics studied in this work. Adapted from [30].

Compounds	Structure
Chlortetracycline (CTC)	
Tetracycline (TC)	
Oxytetracycline (OTC)	
Doxycycline (DC)	

The dramatic increase in the number of species and genera (especially in humans) that have acquired tetracycline resistance as lead to several countries implementing a maximum residue level for this type of antibiotic (**Table 1.2**). [29], [30]

Table 1.2- MRLs for tetracycline group according to Codex Alimentarius. [31]–[33]

Maximum Residual Levels- MRLs (µg/mL)			
Milk (cattle and ship)	Muscle (cattle)	Liver (cattle)	Kidney (cattle)
0.1	0.2	0.6	1.2

1.6 State of the art of TCs detection

Traditionally, antibiotic residues are detected with inhibition tests, mostly agar diffusion tests, such as the Four Plate Test (FPT), but also fast inhibition tests using an indicator for growth. Immunological tests such as enzyme-linked immunosorbent assays (ELISA), solid-phase fluorescence immunoassays (SPFIA) are also used, as well as other analytical methods like liquid chromatography, photoluminescence detection, surface plasmon resonance spectroscopy, voltammetric analysis and electrochemical immunosensors. [27], [29], [31], [34], [35] Most of the mentioned methods are complex, expensive, time consuming or not suitable for field analysis. In this way, it is requested a cheap, easy to perform and rapid analytical method. [36], [37]

Recently was described a colorimetric assay in solution that uses gold nanoparticles plasmon absorption to realize quick detection of TCs at elevated temperature, based on the reaction mechanism of β-Agonists with $HAuCl_4$. TCs showed the capability of directly reducing $HAuCl_4$ into atomic gold, which involved oxidation of the phenol group on the benzene ring, where a quinone-like molecule is formed. [29], [38]

1.6.1 Detection in Milk

TCs are used at the treatment of clinical mastitis and metritis in cow therapy. Failure to discard milk in an appropriate time following lactating cow treatment could result in the presence of this antibiotics in milk, causing harmful effects on consumers. [39]–[43]

As it was said previously, the most used tests for antibiotics are known as microbial inhibitor tests and immune receptor tests. The same applies to its detection in milk. However, they are not specific for antibiotics and there are reports of positive reactions associated with other inhibitors (lactoferrin, lysozyme or sanitisers), leading to increasing demand in the development of new tests for detection of this type of antibiotics in milk. [36], [37], [40], [44]. **Table 1.3** summarizes some tests that are used in antibiotics residues detection in milk (and which are available on the market) and their main characteristics.

The best known test for antibiotics detection in milk is *Delvotest*, whose first version was developed in the 1970s. [40]

Table 1.3- Main characteristics of screening tests for detection of antibiotic residues in milk. Adapted From [45].

Characteristics	**Inhibition of bacterial growth** (*Delvotest, Charm Cowside, Copan*)	**Enzyme immunoassays** (*Charm ROSA, SNAP, BetaStar*)
Analysis time	1 to 3.5 hours	2 to 10 min
Specificity	Nonspecific; broad-spectrum	Specific for one or more antibiotics of a class
Advantages	Broad-spectrum; good beta-lactam detection; low cost	Fast detection; specific for one type of antibiotic
Disadvantages	Nonspecific; slow detection; inhibitor interference	Risk of false negatives
False Positive	Presence of other inhibitors in milk	Cross-reaction with other antibiotics within the same class

Figure 1.3- Some examples of tests that are used in antibiotics residues detection in milk available on the market, and their prices.

<div align="right">Chapter 2</div>

Materials and Methods

2.1 Production Techniques

2.1.1 Synthesis of AuNPs in solution

The experimental method used was based on the study conducted by Shen and his co-workers. [29] The procedure was carried out with hydrogen tetrachloroaurate tri-hydrate (HAuCl_4) 0.2 mM and cetyltrimethylammonium chloride (CTAC) at 2 mM, that was used as a stabilizer.

To a 2 mL eppendorf, it was added 0.5 mL of the above solution, sodium tetraborate buffer (pH 9.2) with a concentration of 0.01 M, and different concentrations (between 1-50 µg/mL) of tetracycline hydrochloride. The eppendorf's were placed in a 70°C water bath for about 15 minutes, thus ensuring the completion of the reaction.

The same procedure was performed for doxycycline hyclate, oxytetracycline hydrochloride and chlortetracycline hydrochloride.

Detailed information about reagents: All reagents are of analytical grade and were used without further purifications. Tetrachloroaurate tri-hydrate from *Acros Organics* (HAuCl_4•$3H_2$O), Cetyltrimethylammonium chloride from *Sigma-Aldrich* ($CH_3(CH_2)_{15}$N$(Cl)(CH_3)_3$), Sodium tetraborate buffer from *Sigma-Aldrich* ($Na_2B_4O_7$, 99%), Tetracycline hydrochloride from *Sigma-Aldrich* ($C_{22}H_{24}N_2O_8$•HCl), Doxycycline hyclate from *Sigma-Aldrich* ($C_{22}H_{24}N_2O_8$•HCl•0,5H_2O•0,5C_2H_6O, ≥98%), Oxytetracycline hydrochloride from *Sigma-Aldrich* ($C_{22}H_{24}N_2O_9$•HCl, ≥95%) and Chlortetracycline hydrochloride from *Sigma-Aldrich* ($C_{22}H_{23}ClN_2O_8$•HCl, ≥75%).

2.1.2 Construction of paper microplates

The construction of paper microplates was made by using the technology Lab-on-Paper and had the following steps: **Preparation of paper substrates** by cutting Whatman nº1 paper sheets and office paper (80 g/cm^2 from *Naviflator*) with the standard size A5 (210 x 148 mm); **Drawing of microplate geometry** using *Adobe Illustrator*. Paper microplates were produced with 96 (diameter of 7 mm) and 384 (diameter of 3.38 mm) wells, with a line width of 0.5 mm and a distance of 1 mm from each other; **Wax printing**, through a *Xerox ColorQube* 8570 printer, whose ink reservoirs have blocks of solid *Xerox* wax. Finally, **diffusion of wax patterns on paper** using a hot plate, heating the paper at 120°C for about 2 minutes.

2.1.3 Colorimetric test on paper

Different series of all reagents were tested on different paper microplates in order to achieve optimization of the process. All reagents used in this stage are the same as in **2.1.1**, except CTAC, which was discarded in this step, since its addition caused a decrease in the intensity of the colour in the paper (**Appendix C**). The procedure with better results was with paper microplate with 384 wells, and has the following steps:

2. Was added to each well, 3 µL of sodium tetraborate buffer at 0.125 M. Again, was allowed to dry at room temperature.

1. 3 µL of gold solution at 0.34 mM was deposited in each well of the paper microplates. Then allowed to dry at room temperature.

3. 3 µL of each of the four different TCs solutions in concentrations between 0.05 and 100 µg/mL was then deposited, leaving to dry again.
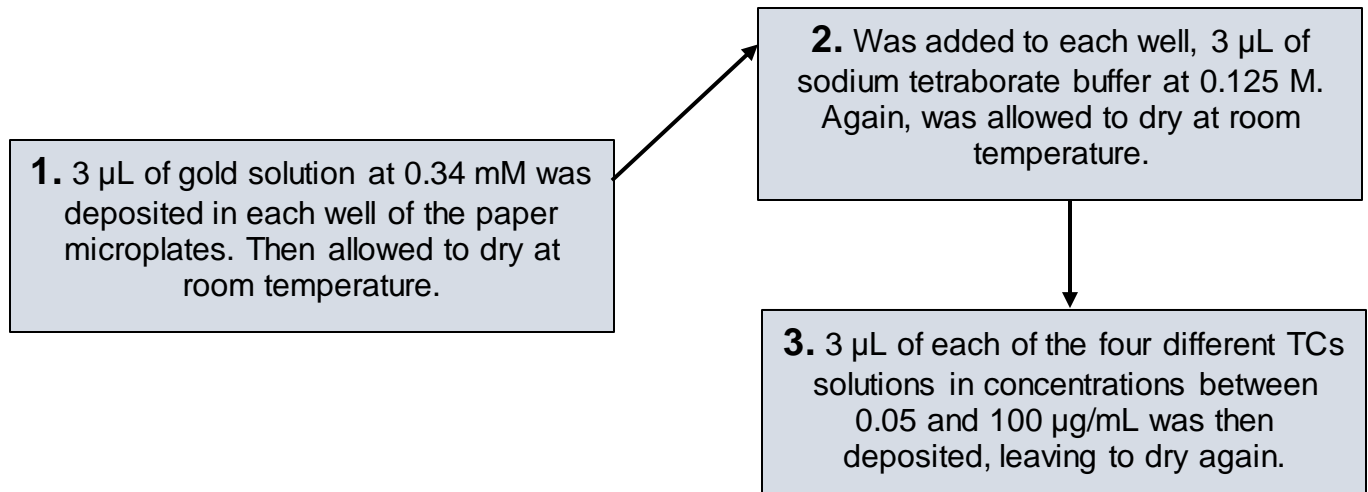
Figure 2.1- Scheme of the experimental procedure of colorimetric tests in paper.

2.1.4 Detection of TCs in milk samples

Various forms of milk treatment were analysed, summarized in table 0.4 in **Appendix J**. Samples from commercially available *Mimosa* UHT milk, (stored at 4°C) were used. The procedure consisted in repeating sections **1.** and **2.** of section **2.1.3**. At the end, 3 µL of the pre-treated milk was deposited with spiked TC concentrations between 0.05 and 20 µg/ml.

2.1.5 Paper-based Biosensor Development

The development of the biosensor essentially involved 3 steps: **Wax printing of the wells and their diffusion** on paper, similar to that referred in section **2.1.2**; **Deposition of the reagents** and their drying, and finally, the **wax printing of the encapsulation layers** (front and back), without their diffusion.

2.2 Characterization Techniques

2.2.1 UV-Vis Spectrophotometry

With the objective of analysing the response of the AuNPs to different concentrations of TCs, the analysis of the solutions by UV-Vis spectrophotometry was performed using TECAN SPARK 10M, incorporated with a High-Speed Monochromater and SparkControl software, for reader control and reduction of data. The AuNPs synthesized on paper were also analysed by UV-Vis spectrophotometry to compare the absorbance spectra of the different wells.

2.2.2 Paper Characterization

To confirm the effectiveness of the paper chosen *(Whatman* nº1- *GE Healthcare*) for the developed biosensor, several characterization techniques were used, such as: Scanning Electron Microscopy (SEM), Energy Dispersive X-ray Spectroscopy (EDS), X-ray Diffraction (XRD) and Fourier-Transform Infrared Spectroscopy (FTIR).

2.2.3 Characterization of AuNPs synthesized on paper

The AuNPs synthesized in paper were observed and characterized (morphology, chemistry and structure) using Scanning Electron Microscopy (SEM), Energy Dispersive X-ray Spectroscopy (EDS) and X-ray Diffraction (XRD).

2.2.4 Digital Analysis

The results were analysed from a desktop scanner (*Cannon* MG5250) and subsequently subjected to an RGB (Red Green Blue) analysis through the *ImageJ* software. In this way it was possible to correlate, in a calibration curve, the analyte's concentration and the intensity of the colour of each well.

<div align="right">Chapter 3</div>

Results and Analysis

3.1 Paper Characterization

In the present work, two types of paper were used as support for colorimetric assays: office paper and Whatman nº1 paper. In this way, it is important to obtain information about the two structural, chemical and morphological properties, thus characterizing the paper types used in the development of the paper sensor.

In addition, in order to show the differences between these supports, it is also important to know some of their macroscopic properties, referred to in **Table 3.1**.

Table 3.1 - Macroscopic properties of Whatman paper and office paper. [3]

Macroscopy Feature	Whatman nº1 Paper	Office Paper
Weight (g/m^2)	88.0	81.3
Thickness (µm)	180	102
Density (kg/m^3)	489	797
Porosity (%)	68	49

It is possible to observe that office paper presents, in relation to Whatman paper, a smaller thickness and a smaller weight. However, it proves to be much denser and consequently less porous.

The greater the density of a given paper, the less space there is between its fibers. The density is then obtained from the ratio of the weight to the thickness of the paper. Knowing this density value, it is also possible to estimate the total pore volume by relating the density of the cellulose fibers (ρ_{fiber}= 1540 kg/m^3) to the paper density, according to **Equation 3.1**.

$$Porosity\ (\%) = \left(1 - \frac{\rho_{paper}}{\rho_{fiber}}\right) \times 100 \qquad \textbf{(3.1)}$$

3.1.1 Scanning Electron Microscopy

In order to observe the surface morphology of the paper substrates used in this study, it was used Scanning Electron Microscopy (SEM). **Figure 3.1** shows SEM images of Whatman paper and office paper.

(A)

(B)
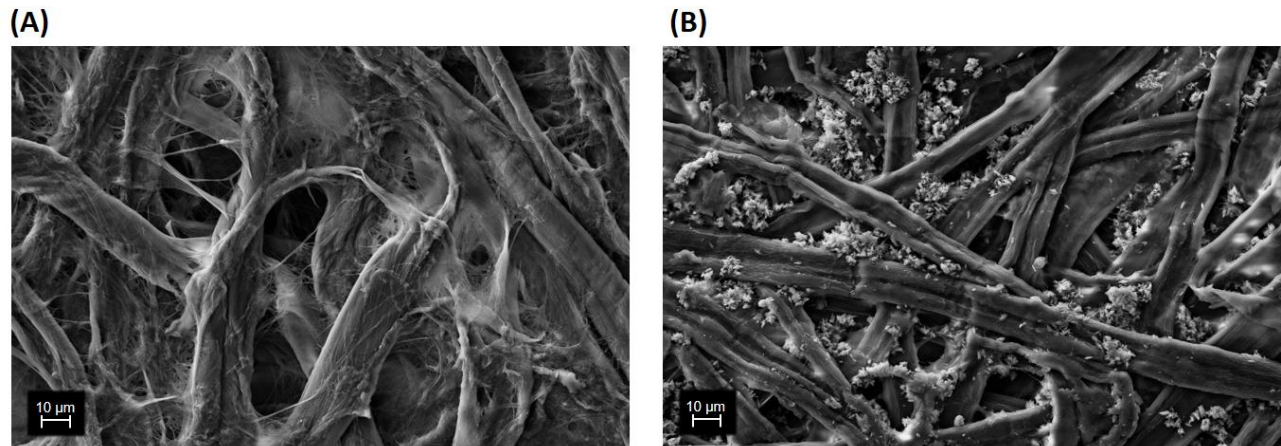
Figure 3.1- Morphology of the paper substrates used. **(A)** SEM image of Whatman paper; **(B)** SEM image of office paper.

Analysing the previous figure, it is possible to observe differences in relation to the morphology of the two paper substrates. In fact, both substrates are mainly composed of a three-dimensional network of cellulose fibers. However, in the SEM image of the office paper, it is observed the presence of small crystalline clusters that possibly correspond to $CaCO_3$, the additive used to give the paper a greater opacity, brightness and whiteness. In addition, it is found that the cellulose fibers in Whatman paper have a cylindrical structure whereas in the office paper these fibers are flatter. This difference in geometry of cellulose fibers gives the Whatman paper a greater thickness.

Also, as expected, lower porosity of the photocopying paper is observed, since the crystalline agglomerates fill most of the pores between the cellulose fibers, thus making the surface of this paper much more uniform than Whatman paper.

3.1.2 Energy Dispersive X-ray Spectroscopy

In order to complement the results obtained by SEM and thus corroborate the existence of $CaCO_3$ (corresponding to the observed crystalline clusters), an elementary analysis was performed by Energy Dispersive X-ray Spectroscopy. It is important, however, to note that this analysis is only capable of detecting the relative elements present, so that alone it is not able to provide all the necessary information to identify all the compounds of a sample.

Figure 3.2 shows the SEM image of the office paper and the corresponding cumulative EDS analysis.
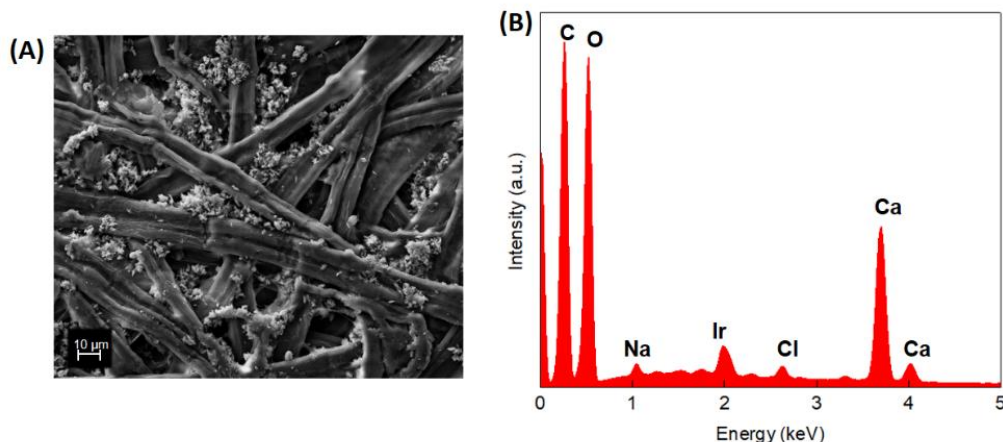
Figure 3.2- EDS analysis of office paper. **(A)** SEM image, **(B)** Cumulative spectrum of EDS analysis of office paper.

In the EDS spectra it is possible to observe that the highest intensity peaks correspond to carbon (E = 0.26 keV), oxygen (E = 0.52 keV) and calcium (in this case there are two peaks for this element, the one with the highest intensity of 3.7 keV, and the lowest intensity peak with energy of 4.0 keV). As expected, the presence of high intensity peaks for carbon and oxygen, reveals the constitution of the largest component in paper, cellulose. However, it is not possible to observe any hydrogen peak (also constituent element of the cellulose), since the EDS technique does not allow to detect this element.

The existence of the characteristic peaks of calcium together with carbon peaks confirms the existence of $CaCO_3$, which corresponds to the clusters observed in SEM images. In addition, three other peaks corresponding to elements in residual amounts were detected: sodium (E = 1.04 keV), iridium (E = 1.52 keV) and chlorine (E = 2.62 keV). The presence of iridium is due to the fact that the conductive coating layer used in the analysed paper substrate was made with this element.

The EDS analysis also allows us to know the distribution of the different elements present in the sample, providing a distribution map obtained through thousands of scans of the electron beam in the area limited by the image. When the detectors signal the presence of a certain element, the software coupled to the equipment adds a white pixel in the zone corresponding to that detection. **Figure 3.3** shows the distribution maps of the main constituents of the office paper.
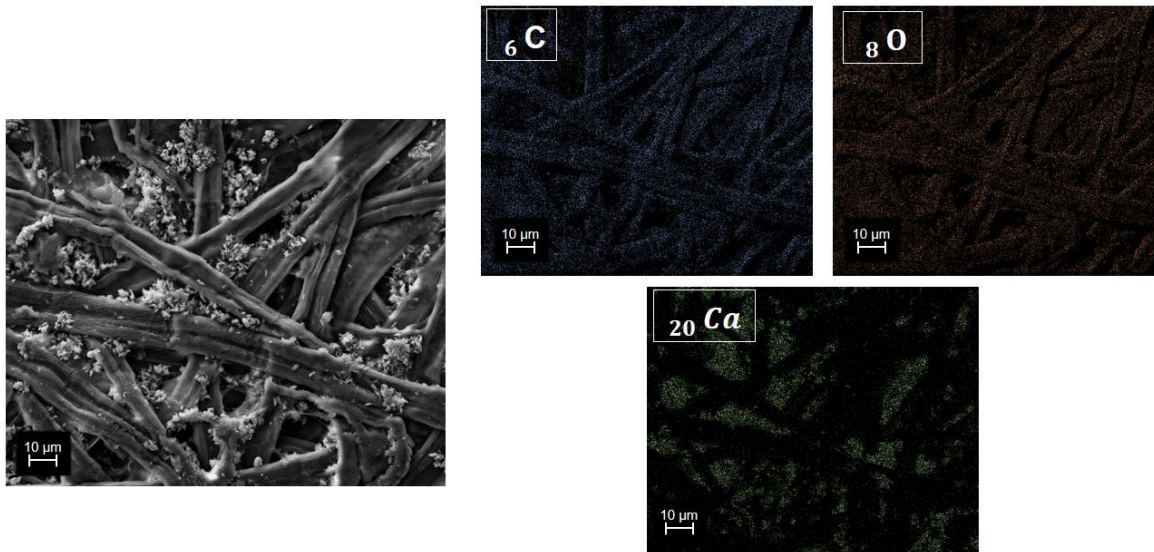
Figure 3.3- EDS map of office paper. The images were artificially coloured in order to facilitate their analysis.

It can be seen from the distribution maps that the main constituents are carbon and oxygen. The calcium element is present in lesser amounts, but still in a considerable proportion. In this way, its distribution map is then in agreement with the presence of the crystalline agglomerates between the cellulose fibers of the office paper.

3.1.3 X-ray Diffraction

The structural analysis of the paper substrates considered was obtained through X-ray Diffraction. The diffractograms as well as the attribution of the identified crystalline structures are represented in **Figure 3.4**.
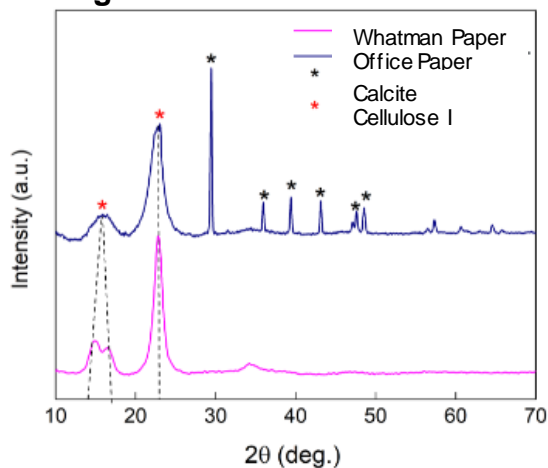
Figure 3.4- Whatman and office paper XRD patterns and crystalline structures identification.

The analysis of the diffractogram allows to verify that both paper substrates have the characteristic peaks of cellulose I. In the case of the Whatman paper diffractogram, two distinct diffraction peaks are observed at 14.92º and 16.46º, while in office paper it can be observed the fusion of these two peaks in only one, at 15.97º. This fusion is because

office paper has residual amounts of various amorphous materials (such as lignin and hemicellulose) in its fibers. In addition to these peaks, these two substrates have yet another common peak, corresponding also to cellulose I, at 22.90º.

As mentioned above, all these peaks are characteristic of cellulose I which has a crystalline structure, and which can be further divided into two other structures, one monoclinic (*Iß* cellulose) and another triclinic (*Iα* cellulose). The sample crystallinity (x_{CR}) is defined as the ratio of the amount of the monoclinic structure to the total amount of sample material. There are several methods for its calculation, one of them is defined as the Segal's empirical method (**Equation 3.2**), which relates the height of 200 peak (peak at 22.90º) and the minimum between the 200 and 110 peaks (peak at 18.00º). However, this method requires that the amorphous material diffracts with the same intensity at 18.00º and 22.90º, and that the crystalline cellulose does not contribute to the intensity at 18.00º. [46]

$$x_{CR} = \frac{I_{200} - I_{AM}}{I_{200}} \qquad (3.2)$$

I_{200} represents both crystalline and amorphous material (peak at 22.90º), while I_{AM} represents only amorphous material ($2\theta = 18º$). [46] It was found that the office paper has a lower crystallinity index (0.7796) than Whatman paper (0.8601).

It is also possible to identify another crystalline structure related to the diffractogram of office paper, which corresponds to calcite ($CaCO_3$), as previously suggested by SEM and EDS results. This crystalline structure has a rhombohedral geometry and is the main additive in the process of making office paper.

3.1.4 Fourier-Transform Infrared Spectroscopy

In order to confirm the presence of the chemical bonds identified by X-ray diffraction, it was used the Fourier-Transform Infrared Spectrocopy (FTIR) technique. The FTIR spectra obtained for the photocopying paper and Whatman paper are in the **Figure 3.5 - (A).**
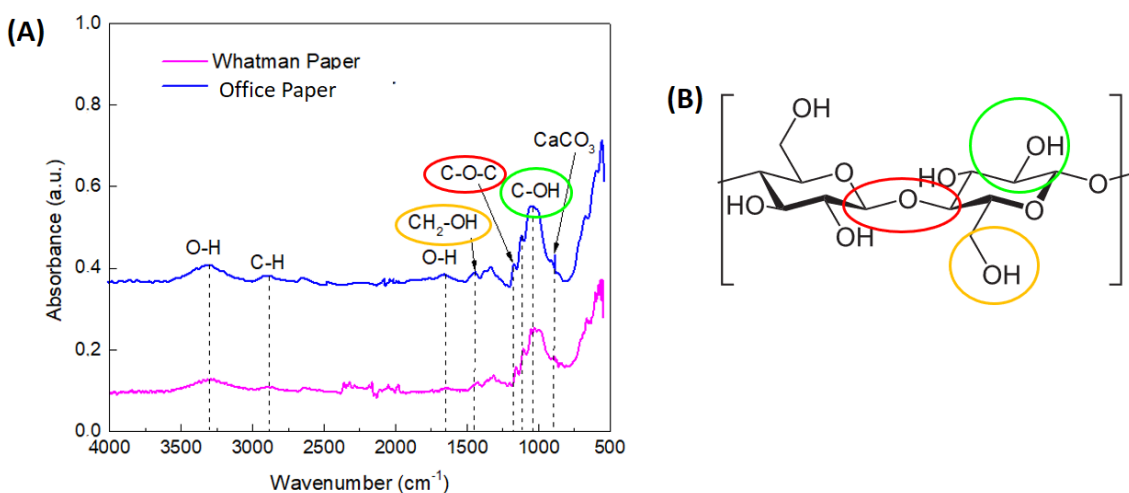
Figure 3.5- Chemical analysis of paper substrates considered. **(A)** FTIR-ATR spectra and identification of the chemical bonds corresponding to the characteristic peaks, **(B)** Chemical structure of cellulose.

15

The range of the 1500-900 cm^{-1} spectrum corresponds to what is termed the fingerprint region, the region where it is possible to identify the characteristic peaks of the cellulose. These are the peaks corresponding to the CH$_2$-OH bonds of the 1433.83 cm^{-1} hydroxyl groups (**Figure 3.5 - (A) and (B)** identified with the orange circle), COC at 1103.10 cm^{-1} (**Figure 3.5 - (A) and (B)** identified with the red circle) and C-OH bonds at 1024.03 cm^{-1} (**Figure 3.5 - (A) and (B)** identified with the green circle). It is also possible to identify the peak at 2898.53 cm^{-1} which corresponds to the C-H bonds present also in the cellulose and a peak at 1155.17 cm^{-1} which corresponds to the asymmetric ring breathing. [47] In addition, the band at 3274.59 cm^{-1} and the peak at 1645.61 cm^{-1} are associated with the O-H vibrations of the water molecules absorbed by the cellulose crystal structure.

In the case of office paper, a peak is recorded that is not present in the Whatman paper spectrum at 871.68 cm^{-1}, associated with CaCO$_3$ and correspond to the symmetric C-O stretching mode. Again, it is possible to confirm the presence of this compound in this type of substrate. Beyond this peak, CaCO$_3$ produces a band at about 1420 cm^{-1} (correspond to the asymmetric C-O stretching mode) and another peak at 712 cm^{-1} (correspond to OCO bending). However, the characteristic cellulose peaks in this zone conceal these regions, preventing their identification. [47]

It is also verified that there is no peak in the region between 1750 and 1500 cm^{-1}, which suggests that characteristic components of this region (such as hemicellulose and lignin), are not found in these substrates. In addition, several peaks in the region between 2000 and 2500 cm^{-1} that can be notable, especially for Whatman paper. However, it is assumed to be noise, probably due to poor sample preparation, since there is no reference for this region to any peak or band associated with cellulose.

3.2 Optimization of the colorimetric test

3.2.1 Synthesis of AuNPs in solution

AuNPs in solution were synthetized by direct reducing of HAuCl$_4$ with TCs, without mediator or seed NPs. This is due to the presence of reducing groups on the benzene ring of this antibiotics group. These reducing groups are phenolic-related groups that are oxidized to their respective quinones (oxidative product) by $AuCl_4^-$ with H$^+$ transfer and AuNPs formation (reaction represented in **Figure 3.6- (E)**). However, this reaction only occurs at elevated temperature, due to the presence of mono phenolic group that showed to be a weaker reducer than that of the polyphenolic compounds. Furthermore, said synthesis is favoured in the presence of an alkaline medium. This occurs because under basic conditions the protons formed from the oxidation of the phenol group can be quickly neutralized by the buffer, favouring, in this way, the advance of the reaction. [29], [38]

Different concentrations (0.1, 1, 2, 5, 10, 20, 30, 40 and 50 µg/mL) of 4 types of tetracyclines were tested. In **Figure 3.6** it is possible to observe the colour changes in AuNPs solutions, for each type of this antibiotic family.
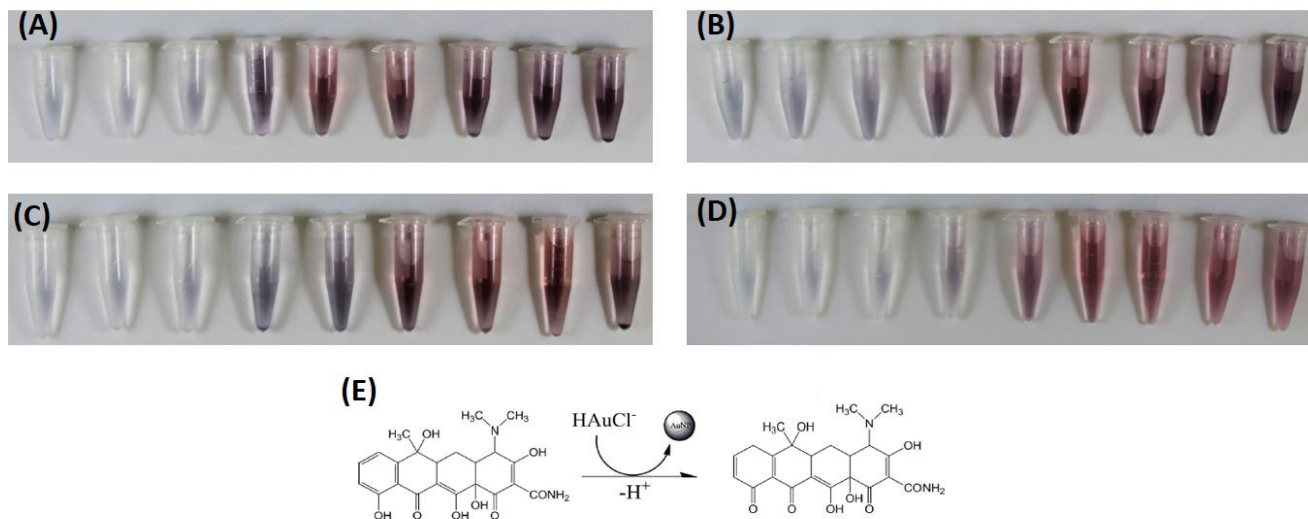
Figure 3.6- Colorimetric differences observed in solutions containing AuNPs synthesized from: **A)** TC, **B)** DC, **C)** OTC and **D)** CTC. **E)** Reaction mechanism between TC and HAuCl₄, adapted from [31].

From the previous figure it is possible to verify that the colours obtained in the solutions with AuNPs are identical for all TCs, indicating that the four TCs have similar reduction activity and substitute group adjacent to the phenol group have little effect on the reaction.

It is also verified that for lower concentrations of the antibiotic (0.1, 1 and 2 µg/mL) the colour obtained is almost imperceptible, since the existing amount of the reducing agent is minimum as compared to the amount of $HAuCl_4$. However, it is possible to observe a blue/purple colour for low concentrations and a pink/red colour for higher concentrations. This colour difference is associated with the size of the AuNPs obtained, with the blue colour representing a larger diameter of NPs, and the red colour being associated with a smaller diameter of NPs.

3.2.1.1 UV-Vis Spectrophotometry

A UV-Vis spectrophotometry analysis was performed to compare the absorbance spectra of the different solutions for each tetracycline. Transparent 96-well polystyrene microplates with flat bottom were used and 200 µl of each solution to be analyzed was deposited in each well. The absorbance reading was performed in the visible region of the electromagnetic spectrum.

Figure 3.7 shows the evolution of the UV-Vis spectrum of AuNPs and the absorbance changes at 526 nm in the presence of different concentrations of TC. The spectrums and trend curves at 526 nm corresponding to the remaining TCs are found in **Appendix A** and **B**. Three replicates were performed for each of the different TCs concentrations tested. In this way, the mean values and standard deviations were later calculated.
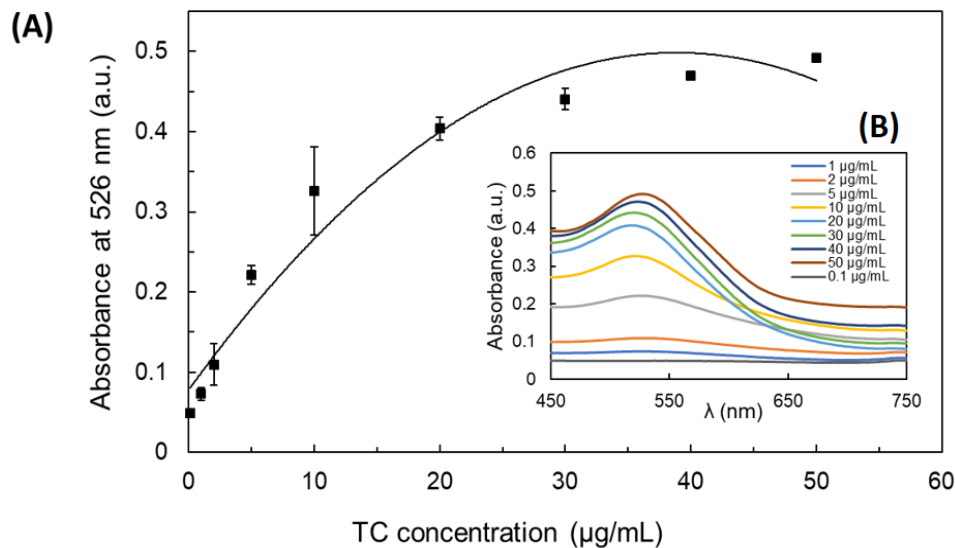
Figure 3.7- (A) Absorbance changes at 526 nm in the presence of different concentrations of TC. **(B)** UV–vis spectra of AuNPs upon addition of **TC.**

From **Figure 3.7 – (B)** it can be seen that the absorbance at 526 nm increases as the concentration of tetracycline increases too. In addition, from about 20 µg/mL, a shift of the SPR band to higher wavelengths is notable, evidently associated with the colour change of the solutions and, in turn, with the size of AuNPs.

In **Figure 3.7 – (A)** the trend curve corresponding to each absorbance point at 526 nm are shown for each concentration of TC under study. It is observable that the absorbance at 526 nm has been shown to have a linear relationship with TC concentrations up until about 10 µg/ml, being that from these concentration values, the curve stabilizes. This behaviour of increasing the absorbance to 526 nm as the concentration of antibiotics increases is called the hyperchromic effect.

3.2.2 Synthesis of AuNPs on paper and TCs quantitation

To guarantee a high signal amplitude, various concentrations of all reactants involved in the reaction were tested. Two types of paper (Whatman and office paper) were also tested, initially from the 96-well microplates. It should be noted that in the initial phase only optimization for tetracycline was carried out. In addition, the use of CTAC was discarded, since its goal is the nanoparticles stabilization in the long term, and the purpose of this sensor is a quick colorimetric analysis at the time of the appearance of the colour. This theory was later tested in an advanced stage of optimization (**Appendix C**).

In **Figure 3.8** it is possible to observe the results obtained for three different concentrations of HAuCl4 and two concentrations of sodium tetraborate buffer, used for nine different concentrations of TC (between 0.05 and 40 µg/mL) in the 96-well microplates in the Whatman and office papers. Columns 1, 2 and 3 represents the control (columns 1 represent only the addition of HAuCl4, columns 2 represent the addition of HAuCl4 plus buffer and columns 3 represents the addition of HAuCl4 and TC). Note that only the wells were filled until line F.

Figure 3.8- Synthesis of AuNPs on paper by reduction with TC, performed on a 96-well microplate on Whatman and Office papers.

It is visible that it was not possible to obtain colour using the same concentrations of HAuCl4 and buffer used in the solution synthesis (line A), thus indicating that they were not sufficient for the effectiveness of the paper reaction. Two more concentration were tested for HAuCl4 and one more for buffer. However, in none of the wells in both papers a colorimetric reaction occurred, again indicating that the chosen concentrations were not sufficient.

The influence of well size was also studied to guarantee the highest sensitivity of the sensor. Thus, 384-well microplates were used, for both papers (**Figure 3.9**). In this case, 13 concentrations of TC were studied (between 0.05 and 100 µg/mL).
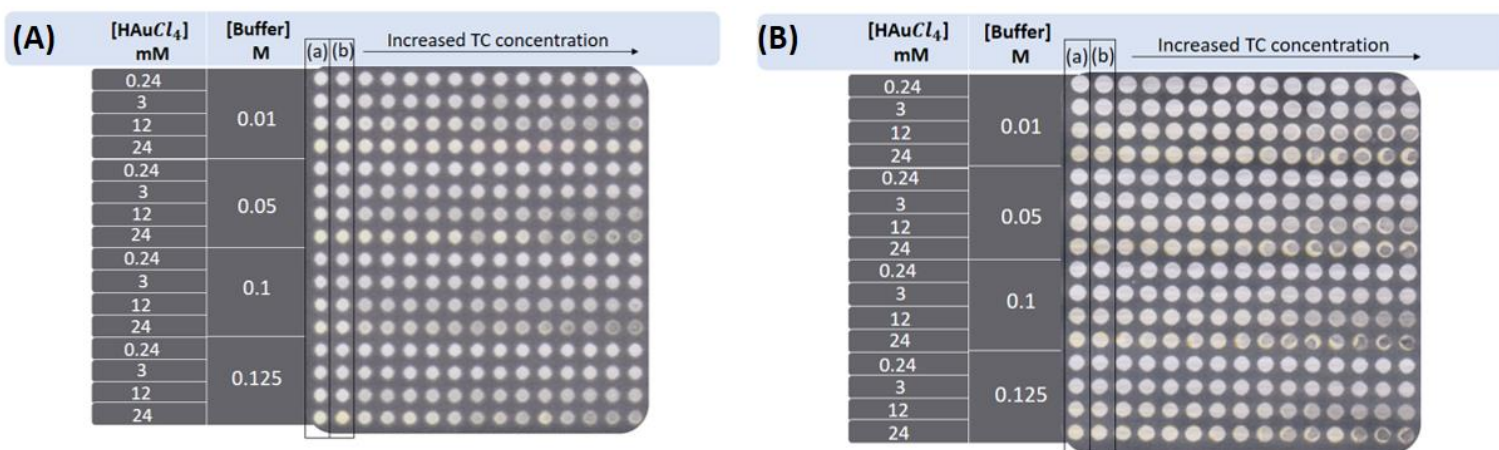
Figure 3.9- Synthesis of AuNPs on paper by reduction with TC, performed on a 384-well microplate on **(A)** Whatman paper and **(B)** Office paper. (a) and (b) columns represents the control.

Analysing the previous figure, it is possible to observe, as before, that the concentrations of HAuCl4 and buffer used in the synthesis in solution, do not allow to obtain colour in both papers. However, unlike 96-well microplates, a slight colour is observed for the remaining concentrations chosen. This is because the size of the wells is smaller in this type of microplate, causing the colour to become more concentrated. For this reason, preference was given to the optimization of the reaction for the 384-well microplates, thus discarding the use of the 96-well microplates.

It is also verified that the colour obtained is not red/pink as spectacle, but rather a medium-grey colour, possibly indicating an AuNPs aggregation. Curiously, it was found

that after about 24h, the colour in the wells changes to red, as can be seen in **Appendix D.** This subject will be discussed in detail after observation of SEM images.

The use of office paper as a substrate for this sensor was discarded, since the colour obtained does not fill the well completely, which may make digital analysis difficult and may influence the achievement of non-uniform results. Furthermore, this paper has the disadvantage of being hydrophobic, which makes absorption of the delay solutions longer than would be desirable in a rapid colorimetric test.

As before, there is no colour appearance for control columns (columns **(b)** in **Figure 3.9** represent only the addition of HAuCl4 and columns **(a)** represent the addition of HAuCl4 plus buffer).

To ensure the appearance of colour for lower TCs concentrations, the concentration of HAuCl4 was further increased up to 34 mM, for 384-well microplate (**Figure 3.10**). The concentration of the buffer was not possible to increase because from 0.15 M the saturation of its solution was reached, and it was not possible to achieve a uniformity of results. The colour of the microplates was modified to a greenish colour to help on the colour visualization by naked eye and guarantee a greater enhancement.

The influence of the volume of solution placed on the wells of the 384-well microplates (**Appendix E**) was also studied, and it was concluded that the volume of solutions that allowed a higher colour intensity was 3 µL.
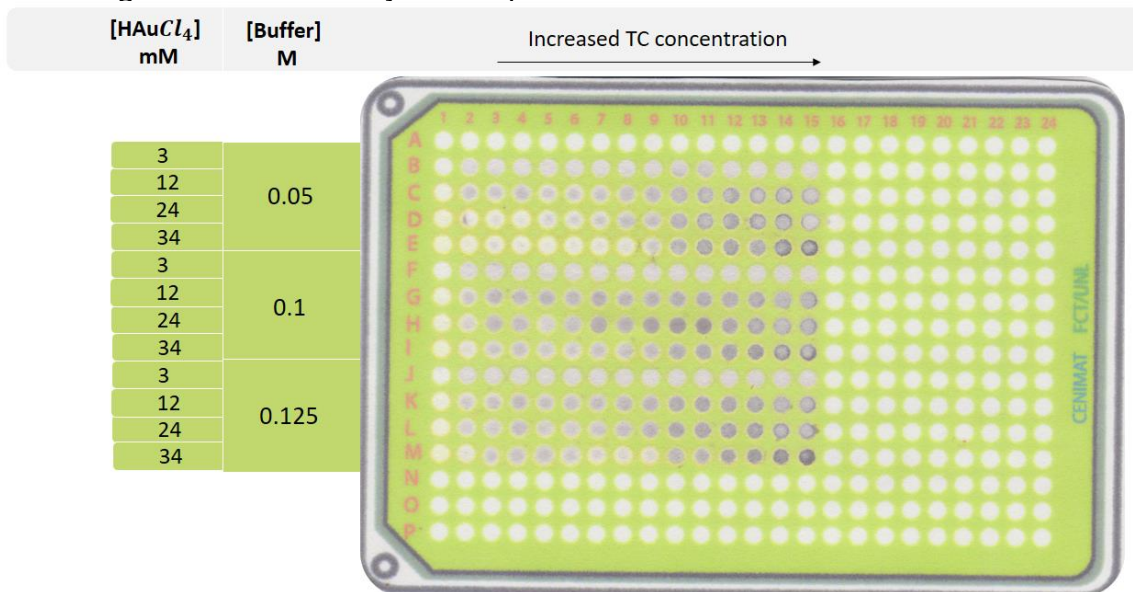
Figure 3.10- Synthesis of AuNPs on Whatman paper by reduction with TC, performed on a 384-well microplate and with deposition of all reagents with a volume of 3 µl. Columns 1 and 2 represent the control.

As for the concentration of HAuCl4, it is found that at 3 mM, for whatever buffer concentration, the colour obtained is always similar, with no increase in colour intensity as the TC concentration increases (lines B, F and J). However, the increase in HAuCl4 concentration corresponds to the increase in colour intensity of the wells. In addition, it is apparent that with increasing HAuCl4 concentration, the wells with lower TC concentration are less filled, indicating that there is not enough TC to reduce the existing amount of HAuCl4. In relation to the buffer concentration, the increase of the colour intensity in the wells is also visible. Another important factor to note is the fact that there is no *coffee ring*

formation (formation of a ring with more intense staining next to the wax barriers), which is an advantage since the formation of this effect harms the correct reading of the intensity of the RGB channels.

To identify more accurately the colour differences occurring as a function of the TC concentration used in the reaction, a digital analysis of the colorimetric results was performed using the *ImageJ* analysis software. The RGB (Red Green Blue) channel intensities were measured for each 384-well microplate test zone. In order to evaluate the intensity of the colour obtained, the arithmetic mean of the three channels was calculated for each test zone. [45] In this way, it is possible to quantify the concentration of the antibiotic to later relate it with the intensity of the colour, in a calibration curve. It is important to mention that the relative intensities of each channel vary between 0 and 255, with 0 corresponding to black and 255 to white. [48], [49]

Three concentrations of $HAuCl_4$ (12, 24 and 34 mM) and two of sodium tetraborate buffer (0.1 and 0.125 M) were used, combined in six different ways, with eight replicates being performed for each combination. This study was performed only for tetracycline. The outliers (values that have a significant distance from the rest of the series to which they belong) were later eliminated in order to reduce the error associated with the measurements. For this purpose, a t-distribution-based method was used, whereby all values that are at a distance from the mean are considered to be greater than 1 standard deviation. In addition, since the number of repetitions is less than 30, this model is the most appropriate to use. [50]

In **Figure 3.11** are represented the trend curves, which relates the average of the three channels with TC concentration. The colorimetric results were obtained for a concentration of sodium tetraborate buffer of 0.125 M, with the different concentrations of $HAuCl_4$ tested. The results corresponding to the RGB analysis performed for each of the combinations tested are presented in **Appendix F**.
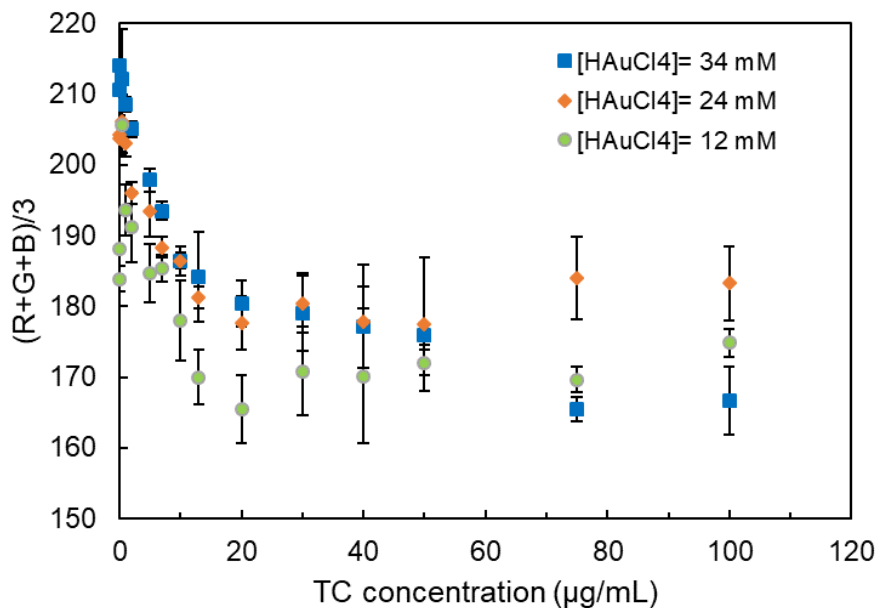

Figure 3.11- RGB analysis of the colorimetric results obtained in the test zones of the microplate of paper of 384 wells. The results presented correspond to a Buffer concentration of 0.125 M with four different concentrations of $HAuCl_4$.

Observing the previous figure, it is possible to verify a decrease in the mean value of the three channels as the TC concentration increases. This may be because the increase in the intensity of the grey colour reveals an approximation of the black colour (whose relative intensity value is 0).

It is also possible to observe that for these combinations represented, the results are very similar, mainly for low concentrations of TC. However, at a concentration of $HAuCl_4$ of 12 mM there is a large dispersion of results, as well as for the concentration of 24 mM from about 20 µg/ml of TC. Thus, based on the results obtained for the different combinations, it is concluded that none of them can independently guarantee a linearity over the entire range of TC concentrations analysed. In this way, it was tried to establish a linearity in the largest possible range of concentrations, using the same concentration of sodium tetraborate buffer (0.125 M) and a concentration of 34 mM for $HAuCl_4$. The same was done for the remaining TCs.

In **Figure 3.12** it is possible to verify that similar results were obtained for all TCs in study.
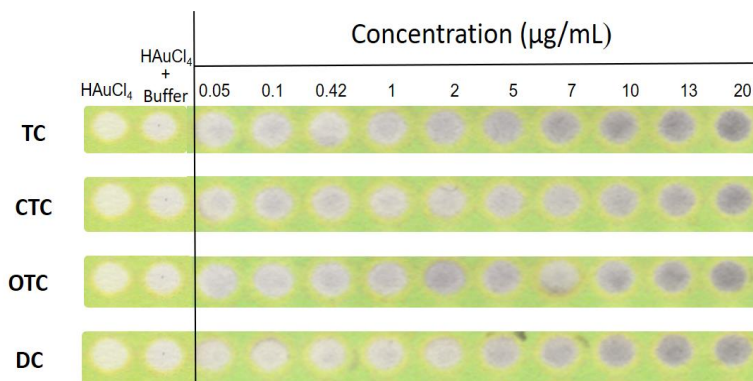
Figure 3.12- Colorimetric results were obtained for all TCs under study with addition of 3 µL of 34 mM $HAuCl_4$, 3 µL Buffer with concentration of 0.125 M, and addition of 3 µL of various concentrations of the different antibiotics. Tests obtained on a 384-well microplate on Whatman paper.

Thus, it is possible to obtain a colorimetric sensor capable of detecting a large range of tetracyclines (four different TCs). However, it is not possible to distinguish between TCs, since the colour obtained for any one of them is quite similar.

In **Figure 3.13** it is possible to observe the four calibration lines for the different TCs. For a better reading of the results and trying to get as close as possible to the straight lines obtained, its normalization was performed in relation to the maximum (214.96) and minimum (197.43) values of mean channel intensity obtained among all TCs (**Figure 3.13 - (B)**). The graphs of the normalized calibration lines for each TC and their line equations are given in **Appendix G**.

(A)

(B)

Figure 3.13- (A) Calibration ratios of the paper sensor considered for the various TCs. **(B)** Normalization of the calibration lines.

A linearity was obtained for all TCs between 0.1 and 10 µg/ml. This interval is sufficient to detect this type of antibiotic in different sample types, since their detected concentration values are usually low. Regarding the detection of this type of antibiotics in milk, it is possible to detect them since the line is linear from the MRL of allowed TCs (0.1 µg/ml). In this way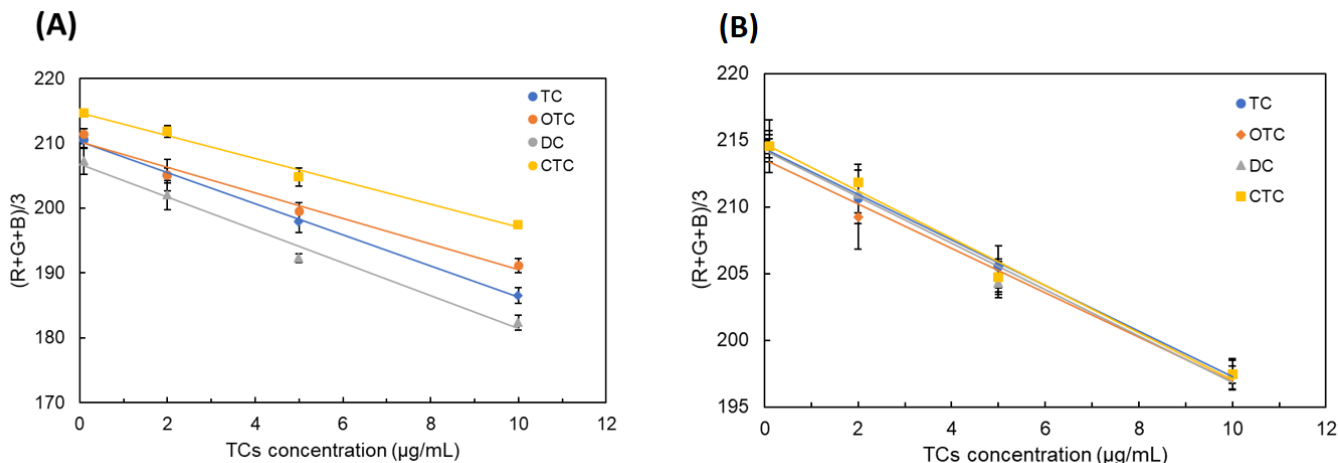, if the RGB analysis of a milk sample corresponds to a value less than 214.96, then it is possible to state that the sample has a tetracycline concentration (whatever the TC present) greater than the maximum allowed value.

It is important to note that if there is more than one type of tetracyclines in the sample, the use of this sensor is no longer feasible, since the existence of a wide variety of TCs at the same time, causes the greater intensity of the colour. However, administration of antibiotics at the same time is not advisable, increasing the risk of adverse drug reactions. [51]

The sensitivity, limit of detection (LOD) and limit of quantitation (LOQ) for each calibration line of the developed sensor was also calculated:

Table 3.2- Sensitivity, LOD and LOQ of each calibration line for all TCs in study.

	TC	DC	OTC	CTC
Sensitivity	-1.712	-1.741	-1.668	-1.770
LOD (µg/ml)	0.789	2.460	1.997	1.774
LOQ (µg/ml)	2.392	7.454	6.050	5.375

Since the calibration lines were performed from a linear regression, it is assumed that the y response of the sensor is linearly related to the concentration x. This relation is expressed by $y = ax + bx$, where the sensitivity is given by b and LOD and LOQ can be represented by:

$$LOD = \frac{3S_a}{b} \qquad \textbf{(3.3)}$$

$$LOQ = \frac{10\,S_a}{b} \qquad\qquad \textbf{(3.4)}$$

S_a is the standard deviation of the response and b is the slope of the calibration curve. The standard deviation of the response can be estimated by the standard deviation of either y-residuals, or y-intercepts, of regression lines. [52]

3.2.2.2 UV-VIS Spectrophotometry

Analogously to what was done for the case of the synthesis of AuNPs in solution, the colorimetric results obtained in the paper microplates were also analysed by UV-Vis spectrophotometry. Measurements were performed using a 384-well microplate in the range of wavelengths between 525 and 750 nm. The absorbance spectra obtained for each of the wells with addition of TC on the paper microplate are shown in the graph of the following figure:
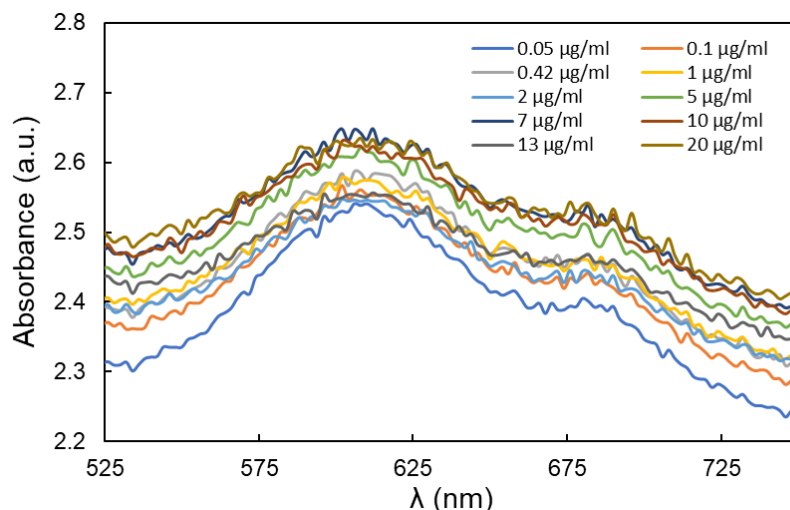
Figure 3.14- Absorbance spectra corresponding to the different wells of the 384 well Whatman paper microplate with TC.

From **Figure 3.14** it is possible to observe two peaks for each absorbance spectrum that suggest the existence of aggregated AuNPs, since a displacement for longer wavelengths corresponds to a larger AuNPs size and the presence of a more bluish/greyish colour.

3.3 Characterization of AuNPs synthesized on paper

3.3.1 Scanning Electron Microscopy

To verify the presence of AuNPs on the surface of the Whatman paper and to observe their morphology, Scanning Electron Microscopy (SEM) was used. The images obtained are presented in **Figure 3.15**, and the images of the paper were observed after deposition and drying of TC, with a concentration of 20 µg/mL (**Figure 3.15 - (A)**) and 24h after this deposition (**Figure 3.15 - (B)**).

Figure 3.15- SEM images of AuNPs synthesized in Whatman paper by reduction with 20 µg/ml of TC. **(A)** Image obtained shortly after TC drying, **(B)** Image obtained after 24h of TC deposition.

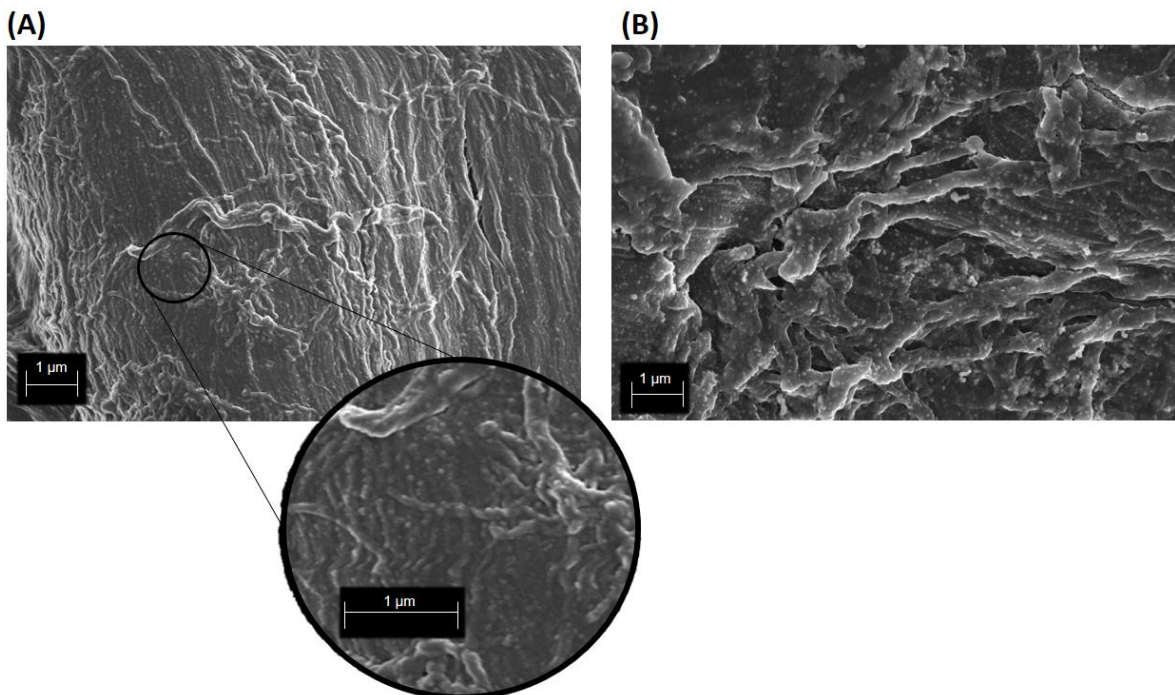Observing the previous images, it is possible to verify that soon after the TC deposition the presence of AuNPs cannot be confirmed, observing only the cellulose fibers that constitute the fibrous network of the paper in question. However, approaching the image it is possible to observe small dots that may correspond to AuNPs of very small dimensions. Due to technical problems with SEM, it was not possible to obtain images with greater magnification. After 24h, when in fact the colour change is observed in the wells, from grey to red, cellulose fibers covered with several bright white dots corresponding to the AuNPs are easily visible, on the same scale.

Thus, the theory previously imposed that the grey colour was due to an aggregation of the AuNPs, is not correct. If it were, in **Figure 3.15 - (A)** we would observe large aggregates of AuNPs, which does not happen. One hypothesis can be supported through the growth mechanism of AuNPs. The formation of AuNPs in an initial state by the Turkevich method is described as the attachment of gold ions in the EDL of the seed particles, obtaining the gray colour through a change of their electronic properties. The fact that the reduction reaction is relatively weak (due to the presence of mono phenolic groups) and the fact that the reaction occurs on paper, between the cellulose fibers, may justify the prolongation of this initial phase of AuNPs formation. [53], [54]

3.3.2 Energy Dispersive X-ray Spectroscopy

To corroborate the previously obtained results, it was used X-ray Dispersive Spectroscopy. The coating was made of carbon to make Au detection possible. The cumulative spectra of the EDS analysis of the Whatman paper, after drying of TC (**Figure 3.16 - (A)**) and after 24h of its deposition (**Figure 3.16 - (B)**), are shown in the following figure.
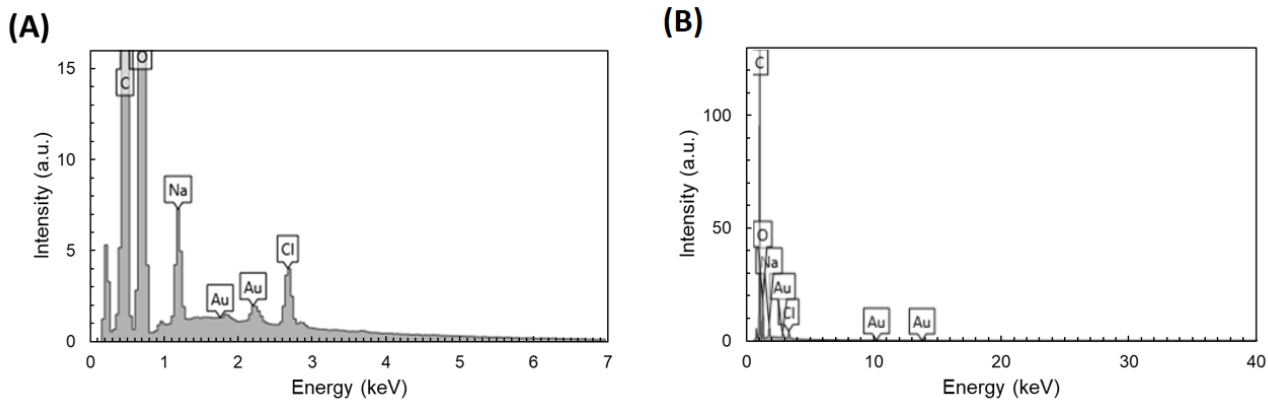
Figure 3.16- Cumulative spectrum for EDS analysis of Whatman paper. **(A)** EDS obtained shortly after TC drying, **(B)** EDS obtained after 24h of TC deposition. The chemical elements present in the sample are identified in the spectrum.

From the spectra of the previous figure it is possible to identify the typical peaks characteristic of the following chemical elements: carbon (E = 0.28 keV), oxygen (E = 0.52 keV), sodium (E = 1.04 keV), chlorine (E = 2.7 keV) and gold (E = 2.12 keV). A further gold peak was detected in **Figure 3.16 - (A)** and two more peaks of the same element in **Figure 3.16 - (B)**, however these can be neglected since they have low intensities. In this way, it was possible to detect in both situations the carbon and oxygen that are the main constituents of the paper fibers, the gold resulting from the reduction reaction of TC for the formation of AuNPs, the sodium that is present due to the addition of sodium tetraborate buffer, and chlorine whose presence can be justified by the formation of $AuCl^-$, after the reaction.

The distribution maps of the main chemical elements present in the samples are presented in **Figure 3.17** and **3.18**.
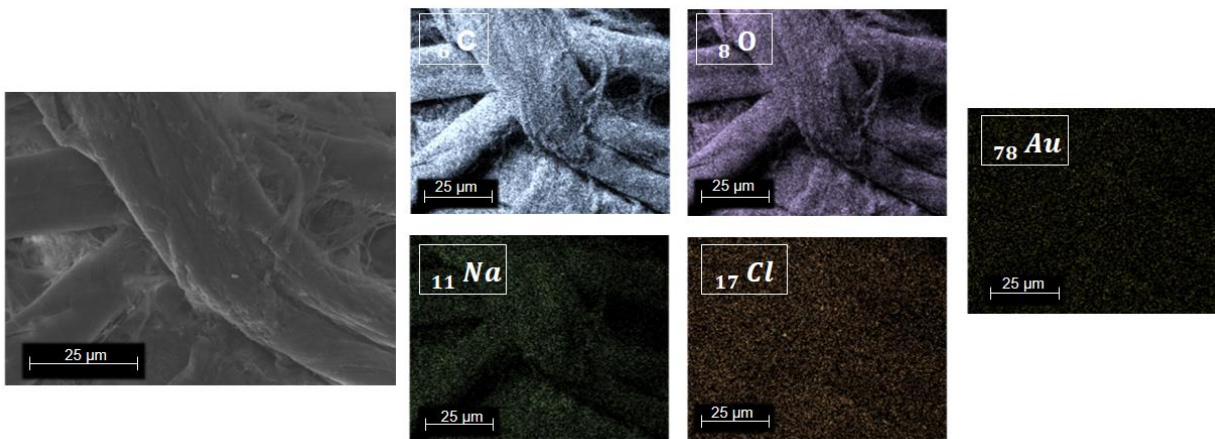

Figure 3.17- SEM image and distribution maps of elements detected in Whatman paper with addition of TC. The images were artificially coloured in order to facilitate their analysis.
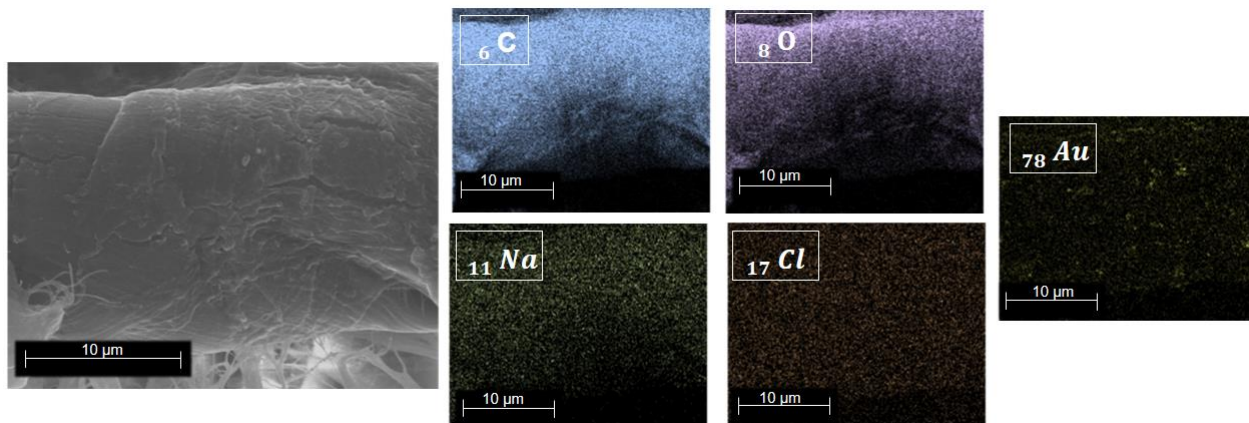
Figure 3.18- SEM image and distribution maps of elements detected on Whatman paper, 24h after addition of TC. The images were artificially coloured in order to facilitate their analysis.

Figure 3.17 concludes that it is not possible to identify AuNPs in Whatman paper right after TC deposition. This may indicate that the small particles previously observed in SEM images may correspond to small crystal particle salts (Na and Cl chemical elements present in the sample) from the buffer used in the experiment. In fact, the presence of these crystals of salts ranging in size from 2-8 nm were observed with reduction of some β-Agonists, like clenbuterol and isoproterenol. [38], [55] These crystals may compromise the identification and observation of AuNPs.

From **Figure 3.18** (corresponding to the addition of TC 24h after its drying) it is possible to identify the presence of gold resulting from the formation of AuNPs. The advanced stage of formation of the gold nanoparticles (which causes the change of colour from gray to red) facilitates their identification.

3.3.3 X-ray Diffraction

In order to complement the results obtained by SEM and EDS, X-ray Diffraction was also used to detect possible crystalline structures on the paper surface.

In **Figure 3.19** it is possible to observe the comparison of the XRD analysis of the Whatman paper without any deposited reagent and right after deposition of $HAuCl_4$, sodium tetraborate buffer and TC.
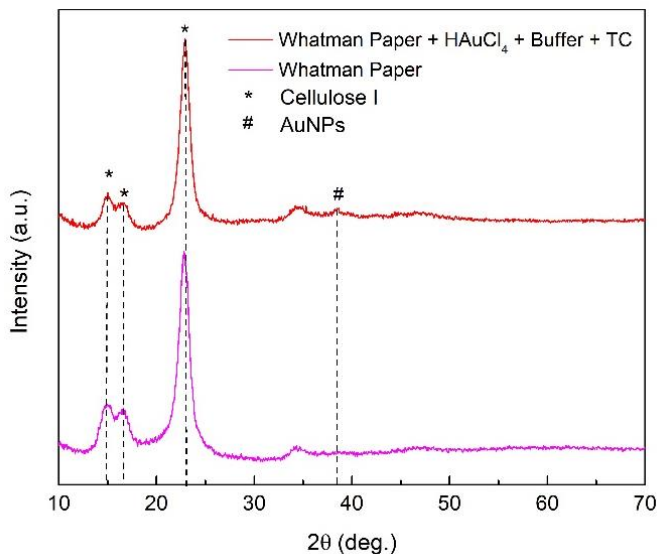
Figure 3.19- Comparison between Whatman paper diffractograms with and without AuNPs formed.

Analysing the represented diffractograms, it is possible to identify a peak around 38.5⁰ referring to the addition of HAuCl₄, buffer and TC in Whatman paper. Although it is visible in relation to the Whatman paper diffractogram, this peak is not very intense, indicating that there are very few AuNPs. This peak is characteristic of the crystalline structure of gold and corresponds to the crystalline plane of the Miller index 111.

3.4 Detection of TCs in milk samples

In order to understand the mechanism of reaction and synthesis of AuNPs with milk as solvent, several forms of milk treatment were studied, to achieve the best optimization of the reduction reaction, which in turn allows the visible colour change detection. Also, these treatments may be essential since TCs have high propensity for forming chelation complexes. For instance, biological matrices contain divalent cations that can interfere with extraction. [56]

In **Appendix H**, all the forms of treatment used, as well as the results obtained for each milk treatment in solution, are described in detail. The AuNPs formation was not possible only with addition of TC to the milk samples. However, it was possible to identify that all forms of treatment of the sample allowed the formation of colour for higher concentrations of TC.

The various forms of milk treatment injected with TC were analysed on Whatman paper, with optimized HAuCl₄ and sodium tetraborate buffer concentrations ([HAuCl₄] = 34 mM and [Buffer] = 0.15 M). The study was again performed only for TC, with the same procedure used in section **2.1.2**.

Concentration (µg/mL)

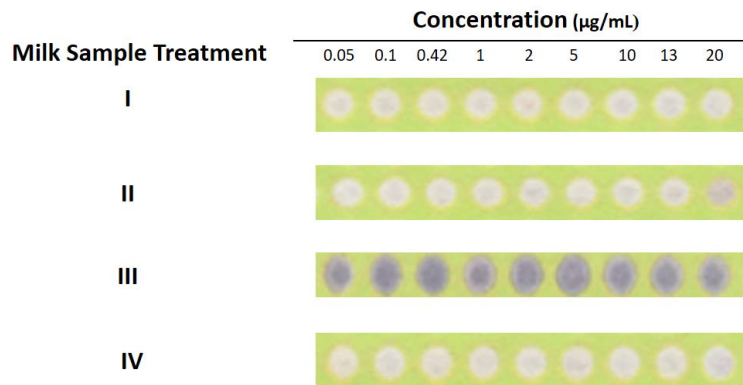Milk Sample Treatment   0.05 0.1 0.42 1 2 5 10 13 20

Figure 3.20- Comparison of the colorimetric results after deposition of milk samples with different concentrations of TC, after different milk sample treatments. Tests obtained on a 384-well microplate on Whatman paper. All the milk sample treatments are described in Appendix H.

From the previous figure it is possible to observe that a greyish colour has been obtained for all TC concentrations and for all forms of milk treatment, thus indicating that it is possible to detect this antibiotic in milk from any of the forms of treatment under study. It is observed that there is a higher colour intensity for treatment III. This colour intensity is due to an interference reaction with the sodium tetraborate buffer, since colour was obtained only with its addition, without TC. Thus, treatment III was discarded as a possible procedure for the treatment of milk samples for the detection of TCs from the developed colorimetric sensor.

However, there is no significant increase in colour intensity for any study treatment. It would therefore be expected that as the concentration in the pre-treated milk sample rises, its colour intensity will increase. In order to confirm what is visible to the naked eye and identify the best form of milk treatment, they were evaluated in order to optimize the sensor developed for the detection of TCs in milk samples.

Three different concentrations of TC were measured using the sensor developed and the results were obtained according to the standard curve obtained for this antibiotic, using the digital analysis. Measurements were replicated three times for each concentration and the standard deviation (SD) were calculated. The results are presented in **Table 3.3**.

Table 3.3- Determination of TC in the pre-treated milk samples. The milk sample treatments are described in Appendix H.

Milk Sample Treatment	Real spiked TC concentration (µg/mL)	Mean of the measured concentrations (µg/mL)	SD (µg/mL)
	0.1	0.49	0.73
I	1	1.0	0.27
	5	0.53	1.26
	0.1	3.02	0.77
II	1	0.11	1.01
	5	1.53	0.86
	0.1	1.17	1.20
IV	1	2.12	0.86
	5	2.97	1.71

From the previous table it is possible to conclude that the treatment IV is what obtains a greater proximity of results in relation to the known concentration spiked in the milk sample. However, an optimization of sensor sensitivity will be a good approach for further studies.

The remaining treatments have widely dispersed results in relation to the known concentration, with no linear relationship. Standard deviations are relatively low, indicating a low dispersion of results for all treatments.

3.5 Development of the final device

Based on the optimizations made, a prototype of the final device was developed for the detection and quantification of TCs, so that it is intuitive, easy to use and accessible to anyone. In **Appendix I** it is possible to observe the final device.

Table 3.4 shows the costs of materials and reagents required for the construction of the device in question. It is important to note that the electricity expenses of the equipment used in the printing process and diffusion of the paper wax standards (wax printer and heating plate) were not considered. Likewise, the deionized water used in the preparation of the reagent solutions is also not included.

Table 3.4- Paper sensor production costs developed for the detection of TCs.

Materials	Quantity	Cost/sensor
Whatman nº1 Paper	4.5×2.5 cm^2	5.96×10^{-3} €
Wax printing	$3 \times (4.5 \times 2.5)$ cm^2	3.15×10^{-4} €
HAuCl$_4$	3 µL= 0.035 mg	0.0021 €
Sodium tetraborate buffer	3 µL= 0.143 mg	9.15×10^{-5} €
TOTAL		0.0085 €

<div align="right">Chapter 4</div>

Conclusion and Perspectives

The present work was focused on the development of a colorimetric paper biosensor for the detection and quantification of four tetracyclines in aqueous solutions and in milk, constituting an alternative to the existing methods. This sensor is based on the synthesis of AuNPs by reduction of HAuCl$_4$ with TCs. After conducting a study of this solution reaction, it was observed that with increasing TCs concentration, there was also an increase in absorbance at 526 nm, revealing a linear relationship up to 10 μg/mL (except for DC, which was up to 20 μg/ml).

The study of the application of colorimetric tests on paper due to its low cost, abundance, availability, biodegradability and easy disposal by incineration, was carried out. Two types of paper were characterized (structural, chemical and morphologically): Whatman n^{0}1 paper and office paper. The type of paper chosen as support for the development of the sensor was Whatman paper, since its properties are much more advantageous in relation to office paper (suitable thickness, porous and hydrophilic).

The construction of the sensors was performed using Lab-on-Paper technology, which consists of the definition of hydrophilic test zones in the paper delimited by hydrophobic regions formed by the impression and diffusion of wax. Several concentrations of each of the reagents were used in the optimization process of the colorimetric detection method on paper. It was observed that the colour obtained was not red as expected, but rather gray, assuming initially that it was due to an aggregation of the AuNPs. From the *ImageJ* software it was possible to calculate the average intensities of the RGB channels of a given test zone. The calibration lines for each of the tetracyclines were obtained based on the arithmetic mean of the three referred channels. All lines have a linear range between 0.1 and 10 μg/ml.

Validation tests of the sensors developed with TC in milk were also performed. It was observed that it is possible to detect this type of antibiotics in pre-treated milk, and four forms of milk treatment were studied. The colour obtained in wells of the microplates in Whatman paper with the samples of TC in milk (concentrations between 0.05 and 20 μg/mL) were similar to those obtained with TC in water. In this sense, and from the obtained calibration lines, it is possible to determine that if a given milk sample with any of the four TCs present has a mean of the RGB channels smaller than 214.96, it has a higher concentration than the permitted one (0.1 μg/mL).

The presence of AuNPs on paper, resulting from the reduction of HAuCl$_4$ with TCs, was studied. It was not possible to confirm the presence of AuNPs in SEM after deposition and drying of TC (discarding the AuNPs aggregation theory). These were only possible to observe 24h after TC deposition, when there was a change of colour from gray to red/pink. However, it was possible to prove their existence in minimal quantities from EDS and XRD. It was posed as a possibility that the origin of the gray colour obtained is due to the weak reduction reaction of HAuCl$_4$ with TC due to the presence of mono phenolic groups. This weak reduction leads to an extension of an initial phase of the AuNPs growth, described as the attachment of gold ions in the EDL of the seed particles, obtaining the grayish/blue colour through a change of their electronic properties.

In this way, it was possible to develop a colorimetric sensor on paper, simple and fast, capable of detecting four types of tetracyclines. This sensor also allows the detection of

TC in pre-treated milk. However, it is not possible to distinguish between TCs and if there is more than one TC present in the sample to be analysed, the results obtained would be ambiguous. It would therefore be interesting to optimize the sensor in this sense. Another aspect to explore would be to perform tests using other types of samples than milk.

In addition, it would be interesting to compare the RGB analysis of digitized results using a scanner and through photography using a smartphone camera, so that it is possible to develop a smartphone application that based on the calibration lines presented allows to perform a quantitative analysis, automatically converting the colour observed in the biosensor test zones to a numerical value of TCs concentration.

Testing other possible geometries for the device, in particular the manufacture of biosensors in 3D format, would also be interesting to address.

<div align="right">

Chapter 5
References

</div>

[1]   M. Ek, G. Gellerstedt, and G. Henriksson, *Paper chemistry and technology*. 2009.

[2]   A. Smook, G, *Handbook for Pulp and Paper Technologists*. 1989.

[3]   A. C. Marques, "Desenvolvimento de um sensor colorimétrico em papel para a deteção de bactérias eletroquimicamente ativas," *Univ. Nov. Lisboa*, p. 115, 2014.

[4]   N. A. Mungroo and S. Neethirajan, "Biosensors for the detection of antibiotics in poultry industry-A Review," *Biosensors*. 2014.

[5]   D. D. M. Sarmishtha GHOSHAL, Debasis MITRA, Sudip ROY, "Biosensors and Biochips for Nanomedical Applications: a Review," *Sensors Transducers J.*, 2010.

[6]   M. P. Ferr, "João Miguel Paitio Ferrão Aplicação da tecnologia de baixo custo Lab - on - Paper a biossensores colorimétricos não enzimáticos para a deteção de glucose," 2017.

[7]   D. D. Liana, B. Raguse, J. Justin Gooding, and E. Chow, "Recent advances in paper-based sensors," *Sensors (Switzerland)*, vol. 12, no. 9, pp. 11505–11526, 2012.

[8]   A. K. Yetisen, M. S. Akram, and C. R. Lowe, "Paper-based microfluidic point-of-care diagnostic devices," *Lab Chip*, vol. 13, no. 12, p. 2210, 2013.

[9]   M. Sajid, A. N. Kawde, and M. Daud, "Designs, formats and applications of lateral flow assay: A literature review," *J. Saudi Chem. Soc.*, vol. 19, no. 6, pp. 689–705, 2015.

[10]   E. M. Fenton, M. R. Mascarenas, G. P. López, and S. S. Sibbett, "Multiplex lateral-flow test strips fabricated by two-dimensional shaping," *ACS Appl. Mater. Interfaces*, vol. 1, no. 1, pp. 124–129, 2009.

[11]   J. Park, J. H. Shin, and J. K. Park, "Pressed Paper-Based Dipstick for Detection of Foodborne Pathogens with Multistep Reactions," *Anal. Chem.*, vol. 88, no. 7, pp. 3781–3788, 2016.

[12]   G. T. Smith *et al.*, "Robust dipstick urinalysis using a low-cost, micro-volume slipping manifold and mobile phone platform," *Lab Chip*, vol. 16, no. 11, pp. 2069–2078, 2016.

[13]   P. Lisowski and P. K. Zarzycki, "Microfluidic paper-based analytical devices (µPADs) and micro total analysis systems (µTAS): Development, applications and future trends," *Chromatographia*, vol. 76, no. 19–20, pp. 1201–1214, 2013.

[14]   A. W. Martinez, "Microfluidic paper-based analytical devices: from POCKET to paper-based ELISA," *Bioanalysis*, vol. 3, no. 23, pp. 2589–2592, 2011.

[15]   M. N. Costa *et al.*, "A low cost, safe, disposable, rapid and self-sustainable paper-based platform for diagnostic testing: Lab-on-paper," *Nanotechnology*, 2014.

[16]   A. W. Martinez, S. T. Phillips, M. J. Butte, and G. M. Whitesides, "Patterned paper as a platform for inexpensive, low-volume, portable bioassays," *Angew. Chemie -*

Int. Ed., 2007.

[17]   J. C. Jokerst, J. A. Adkins, B. Bisha, M. M. Mentele, L. D. Goodridge, and C. S. Henry, "Development of a paper-based analytical device for colorimetric detection of select foodborne pathogens," *Anal. Chem.*, 2012.

[18]   S. K. Ghosh and T. Pal, "Interparticle coupling effect on the surface plasmon resonance of gold nanoparticles: From theory to applications," *Chemical Reviews*. 2007.

[19]   W. Zhao, M. A. Brook, and Y. Li, "Design of gold nanoparticle-based colorimetric biosensing assays," *ChemBioChem*. 2008.

[20]   E. Petryayeva and U. J. Krull, "Localized surface plasmon resonance: Nanostructures, bioassays and biosensing-A review," *Analytica Chimica Acta*. 2011.

[21]   S. Zeng, K.-T. Yong, I. Roy, X.-Q. Dinh, X. Yu, and F. Luan, "AuNP138-A Review on Functionalized Gold Nanoparticles for Biosensing Applications," *Plasmonics*, 2011.

[22]   H. Aldewachi, T. Chalati, M. N. Woodroofe, N. Bricklebank, B. Sharrack, and P. H. Gardiner, "Gold nanoparticle-based colorimetric biosensors," *Nanoscale*, 2017.

[23]   K. Saha, S. S. Agasti, C. Kim, X. Li, and V. M. Rotello, "Gold Nanoparticles in Chemical and Biological Sensing," 2011.

[24]   I. Chopra and M. Roberts, "Tetracycline Antibiotics: Mode of Action, Applications, Molecular Biology, and Epidemiology of Bacterial Resistance," *Microbiol. Mol. Biol. Rev.*, vol. 65, no. 2, pp. 232–260, Jun. 2001.

[25]   M. L. Nelson and S. B. Levy, "The history of the tetracyclines," *Ann. N. Y. Acad. Sci.*, 2011.

[26]   T. H. Grossman, "Tetracycline antibiotics and resistance," *Cold Spring Harb. Perspect. Med.*, vol. 6, no. 4, 2016.

[27]   L. Okerman, S. Croubels, M. Cherlet, K. De Wasch, P. De Backer, and J. Van Hoof, "Evaluation and establishing the performance of different screening tests for tetracycline residues in animal tissues," *Food Addit. Contam.*, 2004.

[28]   J. Li *et al.*, "Simple colorimetric detection of doxycycline and oxytetracycline using unmodified gold nanoparticles," *Opt. Spectrosc.*, vol. 117, no. 2, pp. 250–255, Aug. 2014.

[29]   L. Shen, J. Chen, N. Li, P. He, and Z. Li, "Rapid colorimetric sensing of tetracycline antibiotics with in situ growth of gold nanoparticles," *Anal. Chim. Acta*, vol. 839, pp. 83–90, Aug. 2014.

[30]   I. Chopra and M. Roberts, "Tetracycline Antibiotics: Mode of Action, Applications, Molecular Biology, and Epidemiology of Bacterial Resistance," *Microbiol. Mol. Biol. Rev.*, vol. 65, no. 2, pp. 232–260, 2001.

[31]   J. Zhang, B. Zhang, Y. Wu, S. Jia, T. Fan, and C. Zhang, "Fast determination of the tetracyclines in milk samples by the aptamer biosensor," pp. 2706–2710, 2010.

[32]   FDA and OMS, "LÍMITES MÁXIMOS DE RESIDUOS (LMR) Y

RECOMENDACIONES SOBRE LA GESTIÓN DE RIESGOS (RGR) PARA RESIDUOS DE MEDICAMENTOS VETERINARIOS EN LOS ALIMENTOS CAC/MRL 2-2015 Actualizado en la 38. Sesión de la Comisión del Codex Alimentarius (julio de 2015)," 2015.

[33] C. R. Ec and C. Directive, "European legislation on methods for antibiotics detection in milk," 2002.

[34] S. Chaudhary, S. K. Ali, and Y. P. Singh, "Field method for the micro-quantitative determination of tetracycline in human urine and blood serum," *Orient. J. Chem.*, 2010.

[35] A. L. Cinquina, F. Longo, G. Anastasi, L. Giannetti, and R. Cozzani, "Short communication V alidation of a high-performance liquid chromatography method for the determination of oxytetracycline , tetracycline , chlortetracycline and doxycycline in bovine milk and muscle," vol. 987, pp. 227–233, 2003.

[36] L. He, Y. Luo, W. Zhi, Y. Wu, and P. Zhou, "A colorimetric aptamer biosensor based on gold nanoparticles for the ultrasensitive and specific detection of tetracycline in milk," *Aust. J. Chem.*, 2013.

[37] L. He, Y. Luo, W. Zhi, and P. Zhou, "Colorimetric Sensing of Tetracyclines in Milk Based on the Assembly of Cationic Conjugated Polymer-Aggregated Gold Nanoparticles," *Food Anal. Methods*, 2013.

[38] P. He, L. Shen, R. Liu, Z. Luo, and Z. Li, "Direct detection of ??-agonists by use of gold nanoparticle-based colorimetric assays," *Anal. Chem.*, vol. 83, no. 18, pp. 6988–6995, Sep. 2011.

[39] M. C. Beltrán, R. L. Althaus, A. Molina, M. I. Berruga, and M. P. Molina, "Analytical strategy for the detection of antibiotic residues in sheep and goat?s milk," *Spanish J. Agric. Res.*, vol. 13, no. 1, 2015.

[40] T. F. Microbiologists and R. Road, "MONITORING ANTIBIOTICS IN MILK - THE CHANGING WORLD OF TEST METHODS."

[41] J. W. Fritz and Y. Zuo, "Simultaneous determination of tetracycline, oxytetracycline, and 4-epitetracycline in milk by high-performance liquid chromatography," *Food Chem.*, vol. 105, no. 3, pp. 1297–1301, 2007.

[42] H. Aldewachi, T. Chalati, M. N. Woodroofe, N. Bricklebank, B. Sharrack, and P. H. Gardiner, "Gold nanoparticle-based colorimetric biosensors," *Nanoscale*, 2017.

[43] L. He, Y. Luo, W. Zhi, and P. Zhou, "Colorimetric Sensing of Tetracyclines in Milk Based on the Assembly of Cationic Conjugated Polymer-Aggregated Gold Nanoparticles," *Food Anal. Methods*, vol. 6, no. 6, pp. 1704–1711, 2013.

[44] K. Ai, Y. Liu, and L. Lu, "Hydrogen-bonding recognition-induced color change of gold nanoparticles for visual detection of melamine in raw milk and infant formula," *J. Am. Chem. Soc.*, vol. 131, no. 27, pp. 9496–9497, Jul. 2009.

[45] "Controle de resíduos de antimicrobianos no leite | Ourofino Saúde Animal." [Online]. Available: https://www.ourofinosaudeanimal.com/ourofinoemcampo/categoria/artigos/control e-de-residuos-de-antimicrobianos-no-leite/. [Accessed: 03-Sep-2018].

[46] A. Thygesen, J. Oddershede, H. Lilholt, A. B. Thomsen, and K. Ståhl, "On the determination of crystallinity and cellulose content in plant fibres," *Cellulose*, vol. 12, no. 6, pp. 563–576, 2005.

[47] V. Causin, C. Marega, A. Marigo, R. Casamassima, G. Peluso, and L. Ripani, "Forensic differentiation of paper by X-ray diffraction and infrared spectroscopy," *Forensic Sci. Int.*, vol. 197, no. 1–3, pp. 70–74, 2010.

[48] A. W. Martinez, S. T. Phillips, G. M. Whitesides, and E. Carrilho, "Diagnostics for the developing world: Microfluidic paper-based analytical devices," *Anal. Chem.*, 2010.

[49] M. Q. do N. Costa, "Desenvolvimento de Microfluídica em Papel para Utilização em Biossensores," p. 99, 2012.

[50] "T-Score vs. Z-Score: What's the Difference? - Statistics How To." [Online]. Available: http://www.statisticshowto.com/probability-and-statistics/hypothesis-testing/t-score-vs-z-score/. [Accessed: 21-Aug-2018].

[51] G. Ziv, M. Agriculture, P. O. Box, and B. Dagan, "T h e r a p e u t i c U s e of A n t i b i o t i c s in Farm Animals The prevention and therapeutic management of disease conditions caused by infectious agents are daily events in the practice of farm animal medicine and surgery . Antimicrobial drugs rep," pp. 8–22, 1986.

[52] A. Shrivastava and V. Gupta, "Methods for the determination of limit of detection and limit of quantitation of the analytical methods," *Chronicles Young Sci.*, vol. 2, no. 1, p. 21, 2011.

[53] J. Kimling, M. Maier, B. Okenve, V. Kotaidis, H. Ballot, and A. Plech, "Turkevich method for gold nanoparticle synthesis revisited," *J. Phys. Chem. B*, vol. 110, no. 32, pp. 15700–15707, 2006.

[54] J. Polte, "Fundamental growth principles of colloidal metal nanoparticles - a new perspective," *CrystEngComm*, vol. 17, no. 36, pp. 6809–6830, 2015.

[55] M. Tran, R. DePenning, M. Turner, and S. Padalkar, "Effect of citrate ratio and temperature on gold nanoparticle size and morphology," *Mater. Res. Express*, vol. 3, no. 10, pp. 1–10, 2016.

[56] C. R. Anderson, H. S. Rupp, and W. H. Wu, "Complexities in tetracycline analysis - Chemistry, matrix extraction, cleanup, and liquid chromatography," *J. Chromatogr. A*, vol. 1075, no. 1–2, pp. 23–32, 2005.

[57] M. Jeon, J. Kim, K. J. Paeng, S. W. Park, and I. R. Paeng, "Biotin-avidin mediated competitive enzyme-linked immunosorbent assay to detect residues of tetracyclines in milk," *Microchem. J.*, vol. 88, no. 1, pp. 26–31, 2008.

[58] C. Conjugated, P. G. Nanoparticles, L. He, Y. Luo, W. Zhi, and P. Zhou, "Colorimetric Sensing of Tetracyclines in Milk Based on the Assembly of Colorimetric Sensing of Tetracyclines in Milk Based on the Assembly of Cationic Conjugated Polymer-Aggregated Gold Nanoparticles," no. May, 2016.

[59] Y. Luo *et al.*, "A novel colorimetric aptasensor using cysteamine-stabilized gold nanoparticles as probe for rapid and specific detection of tetracycline in raw milk," *Food Control*, vol. 54, pp. 7–15, 2015.

<div align="right">Appendix</div>

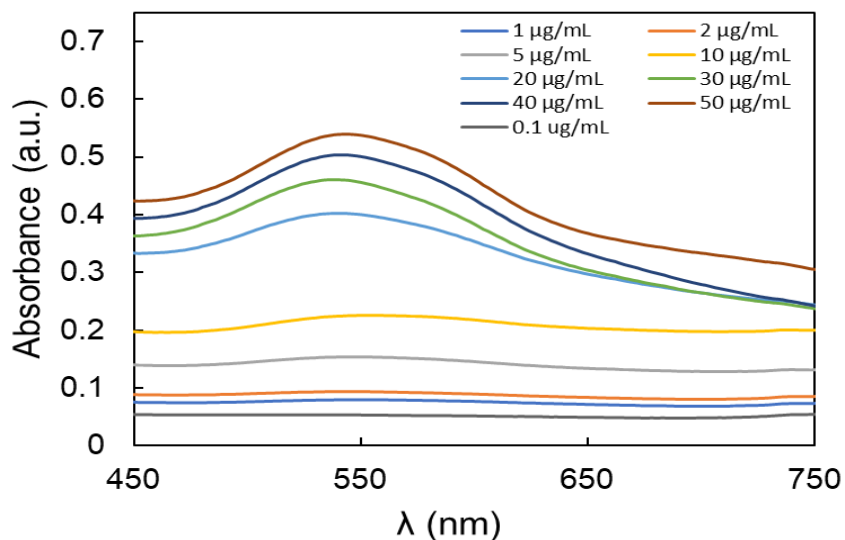## A – UV–vis spectra of AuNPs upon addition of TCs

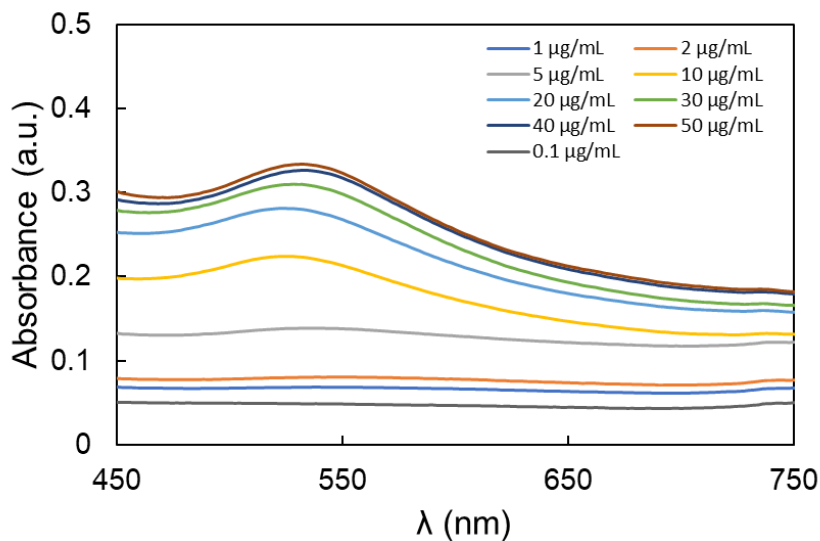**Figure 0.1** - UV–vis spectra of AuNPs upon addition of DC.

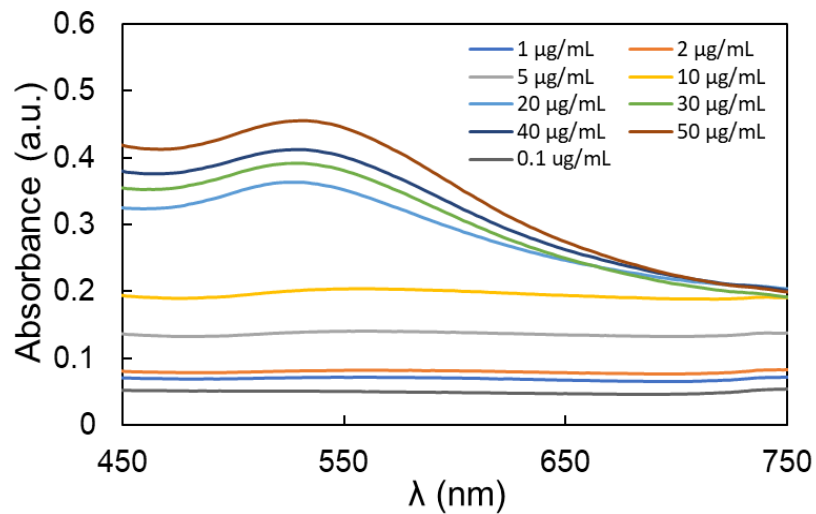**Figure 0.2** - UV–vis spectra of AuNPs upon addition of OTC.

Figure 0.3- UV–vis spectra of AuNPs upon addition of CTC.

The results indicate that the four TCs have similar reduction activity and substitute group adjacent to the phenol group have little effect on the reaction.

B - Absorbance changes at 526 nm in the presence of different concentrations of TCs
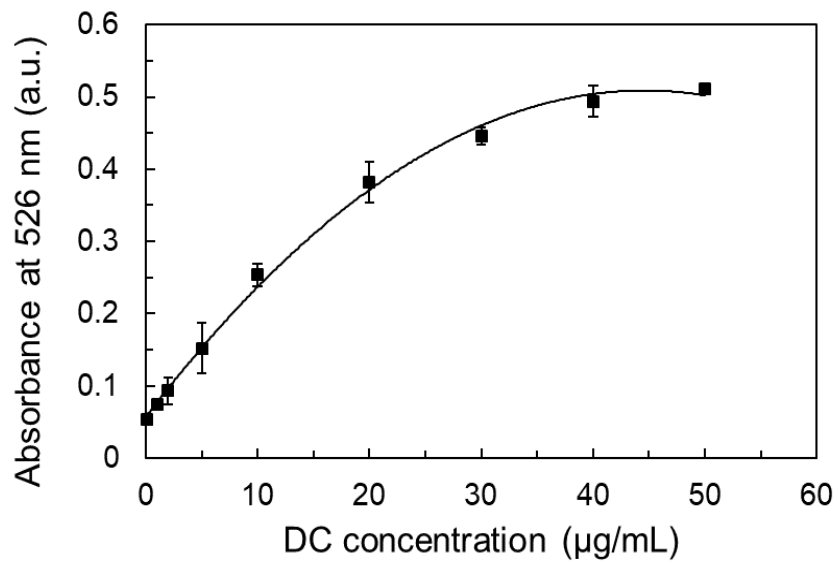
Figure 0.4- Absorbance changes at 526 nm in the presence of different concentrations of DC.
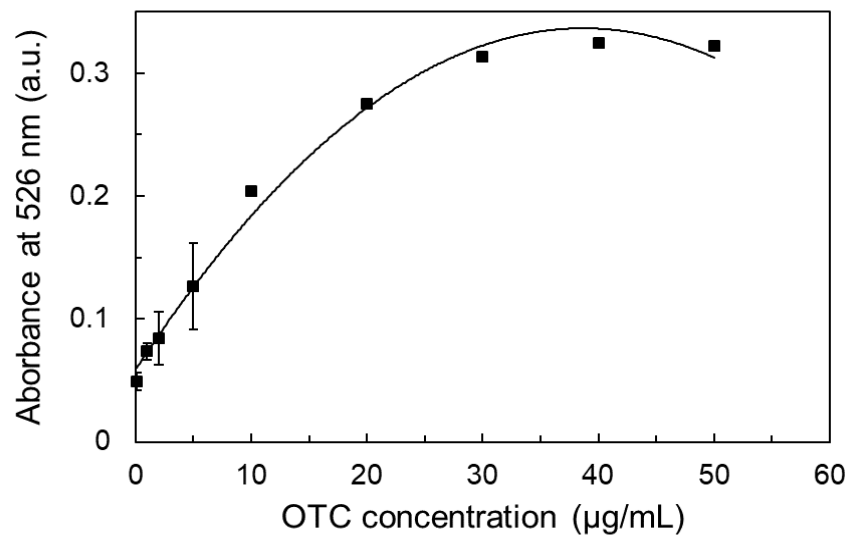
Figure 0.5- Absorbance changes at 526 nm in the presence of different concentrations of OTC.
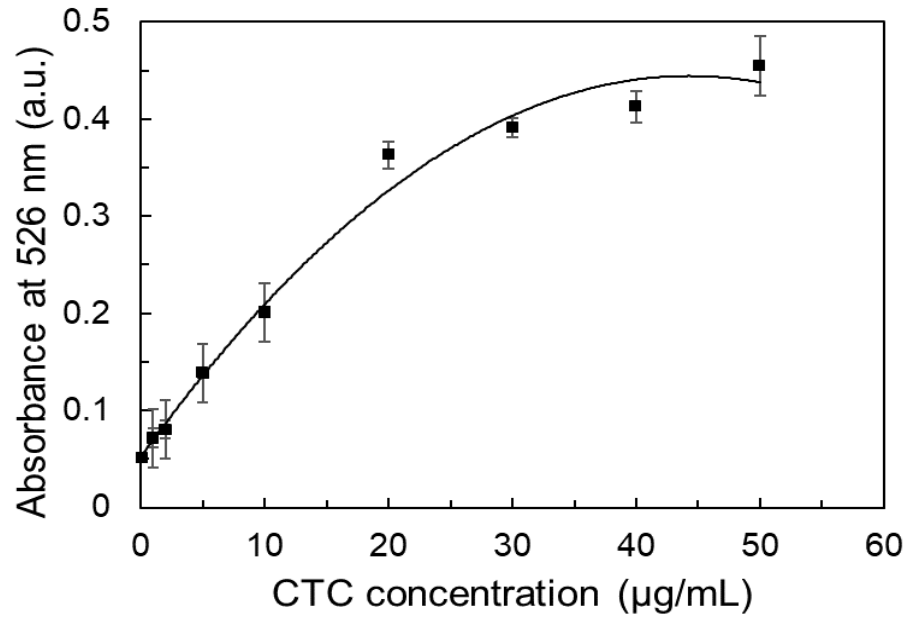
Figure 0.6- Absorbance changes at 526 nm in the presence of different concentrations of CTC.

C - Influence of the addition of CTAC to the reaction on Whatman paper

This study was carried out at an advanced stage of optimization with the addition of 3 µl of $HAuCl_4$ at a concentration of 34 mM and of 3 µL Buffer at a concentration of 0.125 M. Two concentrations of CTAC were tested: 2 mM (Line A) and 4 mM (Line C). For both lines the volume of CTAC placed was also 3 µl. The final solution to be placed was TC (3 µL), with concentrations between 0.05 and 100 µg/mL. Columns 1 and 2 represent the control.

As expected, no momentary colour change was obtained. In fact, there was a decrease at the colour intensity and only the initial colour remaining for more days, which indicates the non-aggregation of the nanoparticles over time with addition of CTAC. It was also observed that the increase in CTAC concentration prevented colour production at low TC concentrations.
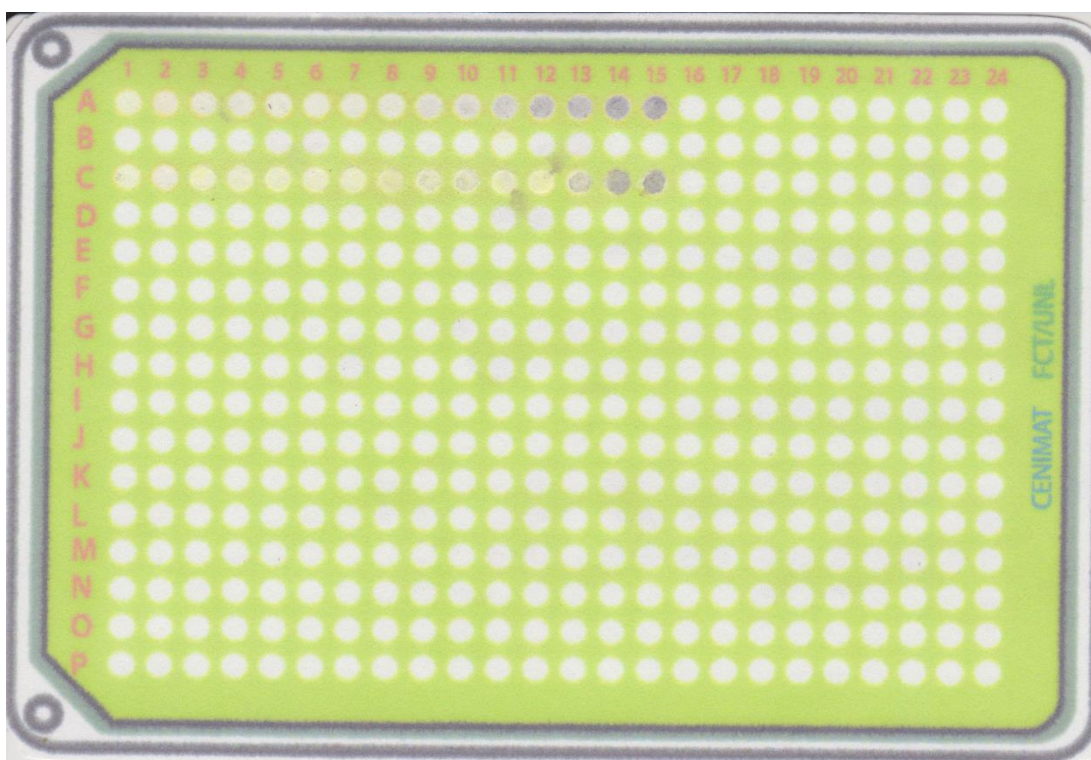
Figure 0.7- Influence of the addition of CTAC to the reaction, in Whatman paper. Line A represents the addition of 2 mM of CTAC and Line C represents the addition of 4 mM of the same reagent.

D - Colour change of the well microplates after 24h of TC deposition
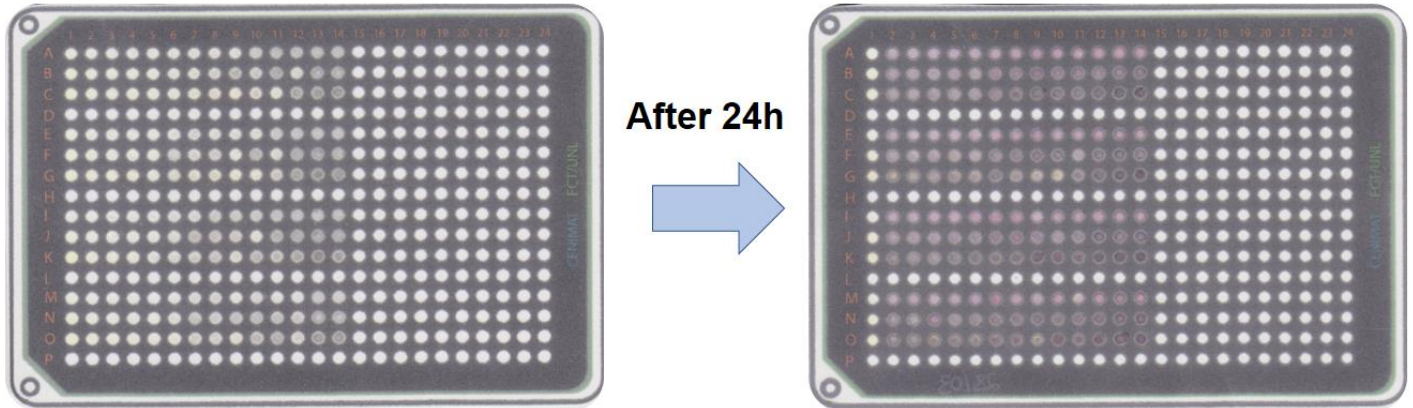
After 24h

Figure 0.8- Colour change (grey to red) of the well microplates after 24h of TC deposition.

From the previous figure it is possible to observe a significant colour change in the wells after 24 hours of the deposition of all the reagents.

Since the purpose of this sensor is the rapid detection of this type of antibiotics, and since a visible colour change after drying of the reagents is obtained, preference was given to optimizing the sensor from the obtained grey colour.

E – Influence of the volume of solutions placed on the wells of the 384-well microplates in Whatman paper
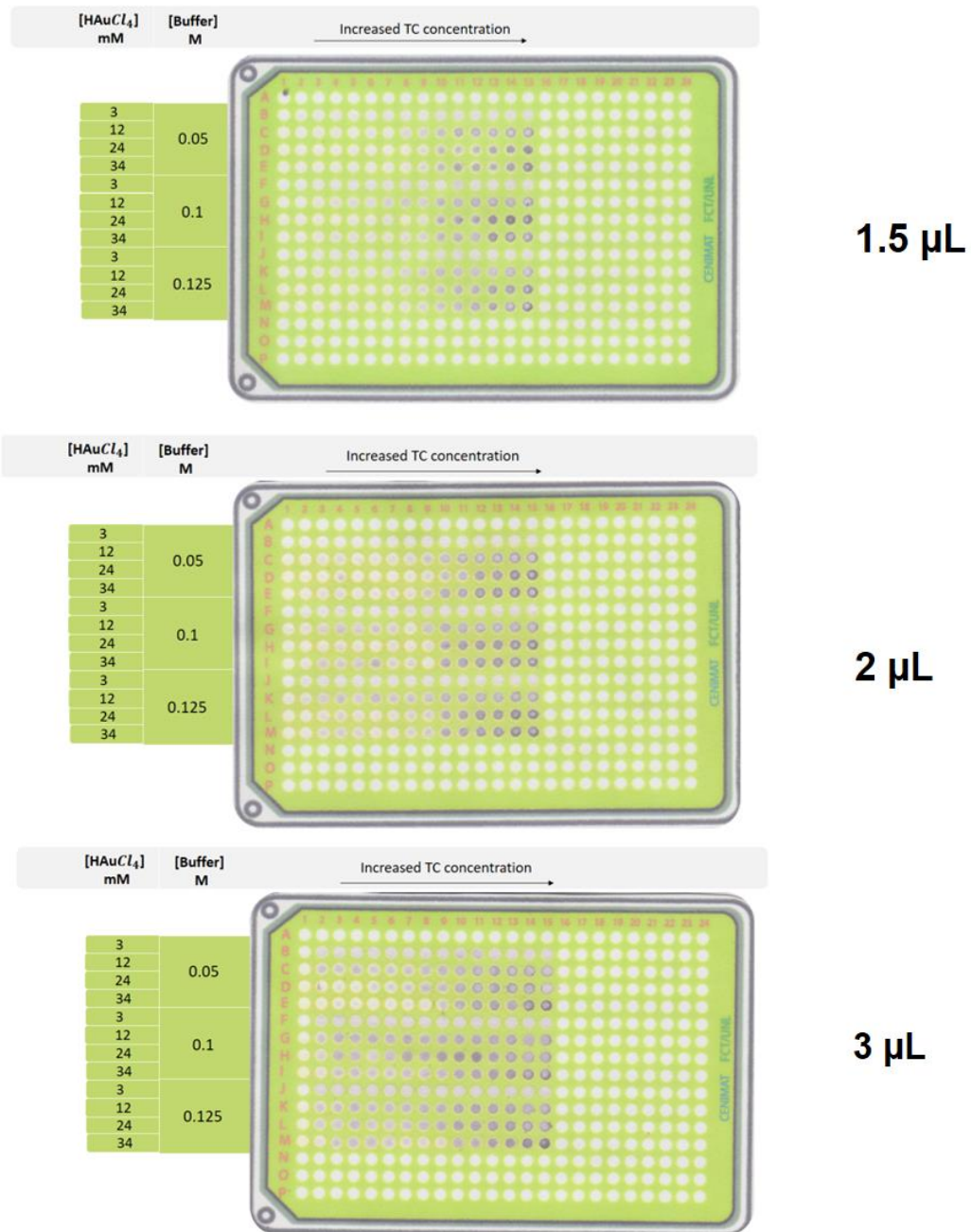
Figure 0.9- Influence of the volume of solutions placed on the wells of the 384-well microplates in Whatman paper. Columns 1 and 2 are the control.

F - RGB analysis for optimization of reagent concentrations used in the process of AuNP synthesis on paper with TC reduction using 384-well microplates on Whatman nº1 paper
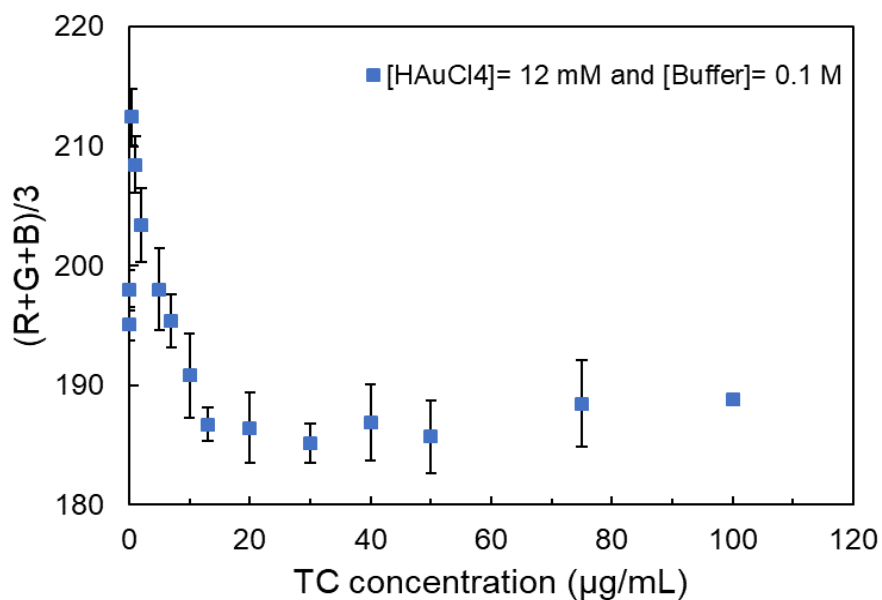
Figure 0.10- RGB analysis of the colorimetric results obtained in the test zones of the microplates, corresponding to a concentration of $HAuCl_4$ of 12 mM and the sodium tetraborate buffer concentration of 0.1 M.
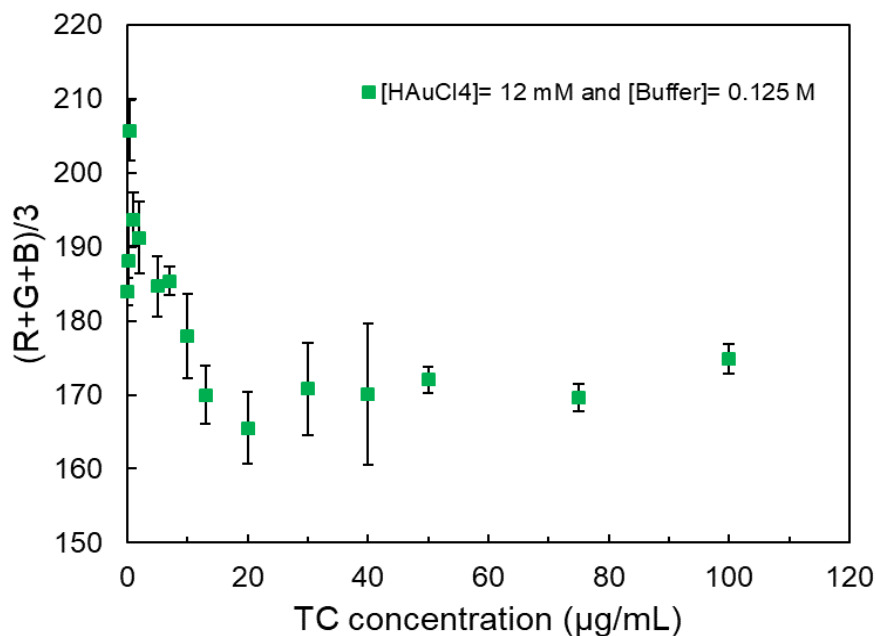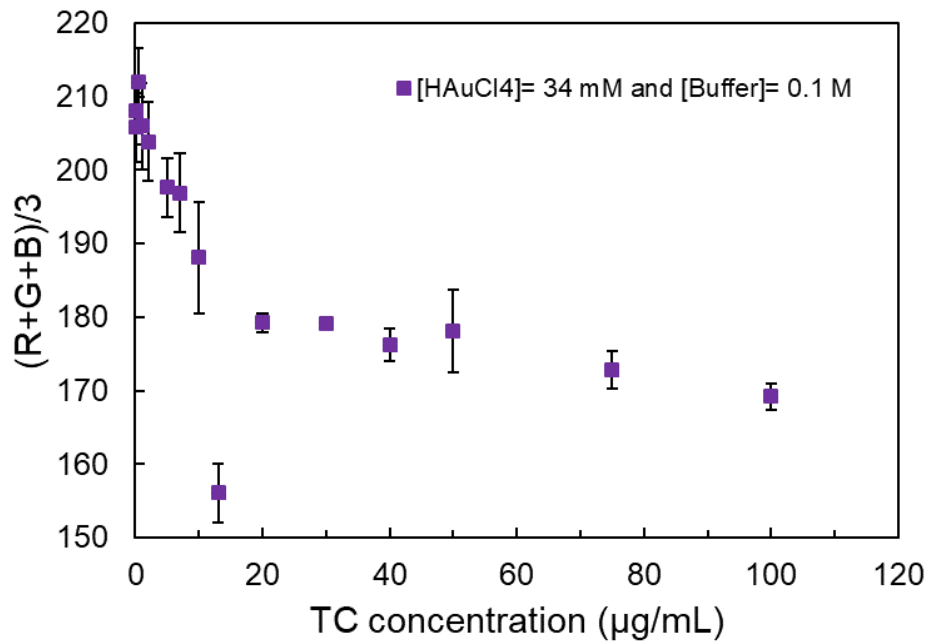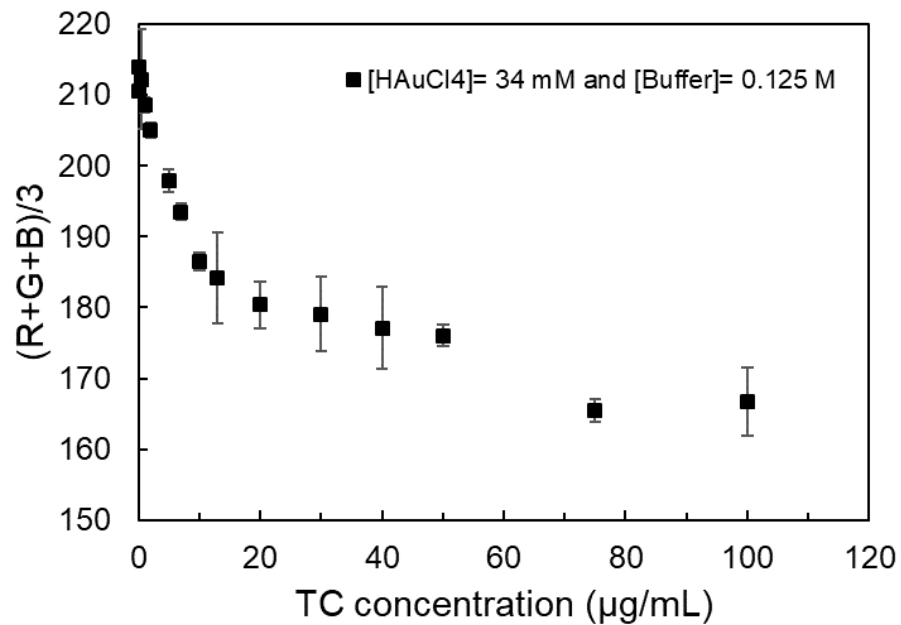

Figure 0.11- RGB analysis of the colorimetric results obtained in the test zones of the microplates, corresponding to a concentration of $HAuCl_4$ of 12 mM and the sodium tetraborate buffer concentration of 0.125 M.
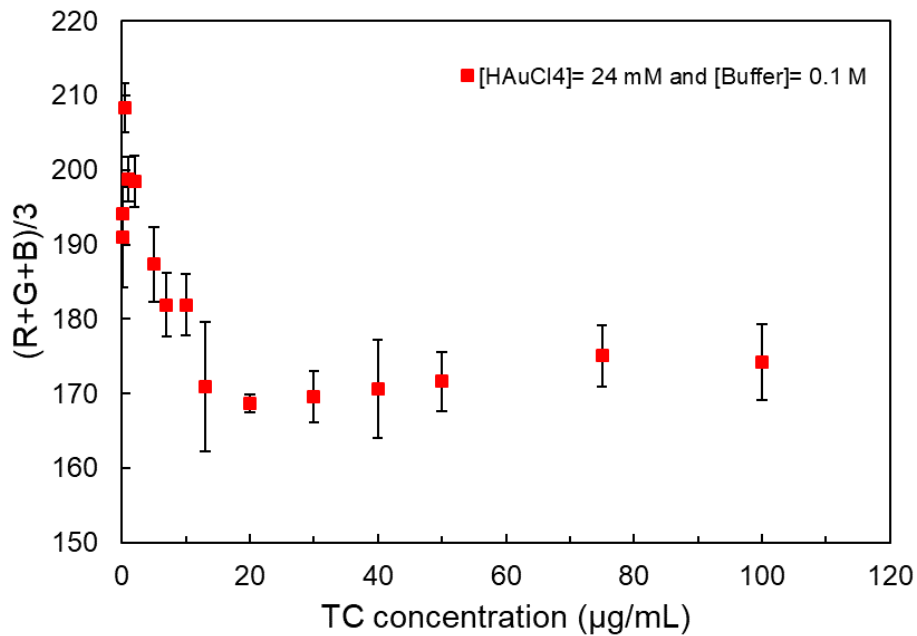
Figure 0.12- RGB analysis of the colorimetric results obtained in the test zones of the microplates, corresponding to a concentration of $HAuCl_4$ of 24 mM and the sodium tetraborate buffer concentration of 0.1 M.
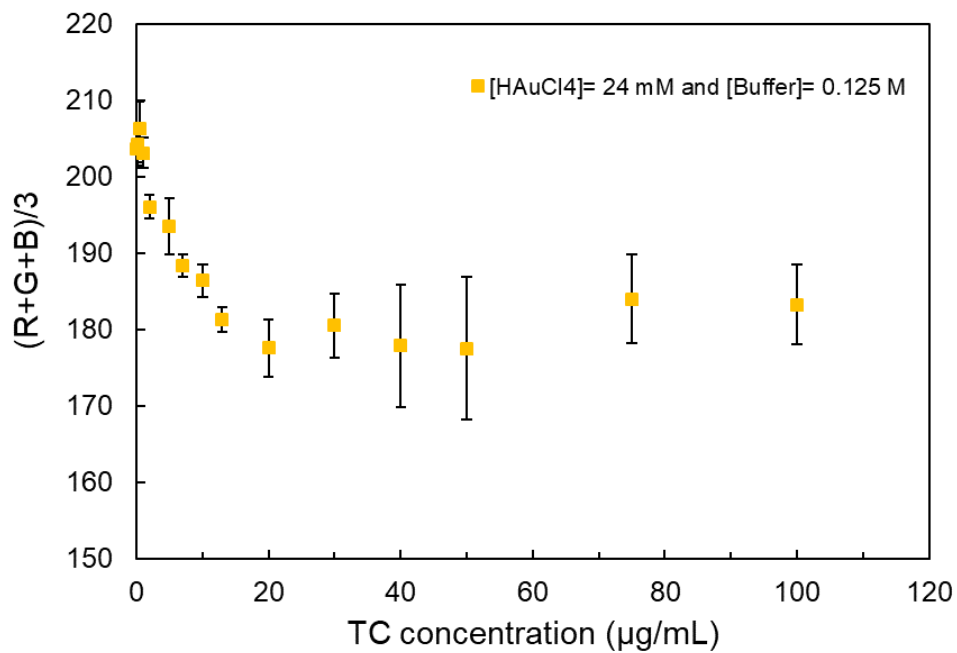
Figure 0.13- RGB analysis of the colorimetric results obtained in the test zones of the microplates, corresponding to a concentration of $HAuCl_4$ of 24 mM and the sodium tetraborate buffer concentration of 0.125 M.

Figure 0.14- RGB analysis of the colorimetric results obtained in the test zones of the microplates, corresponding to a concentration of HAuCl$_4$ of 34 mM and the sodium tetraborate buffer concentration of 0.1 M.

Figure 0.15- RGB analysis of the colorimetric results obtained in the test zones of the microplates, corresponding to a concentration of HAuCl$_4$ of 34 mM and the sodium tetraborate buffer concentration of 0.125 M.

G - Normalized calibration lines for each TC and their Sensitivity, LOD and LOQ determination
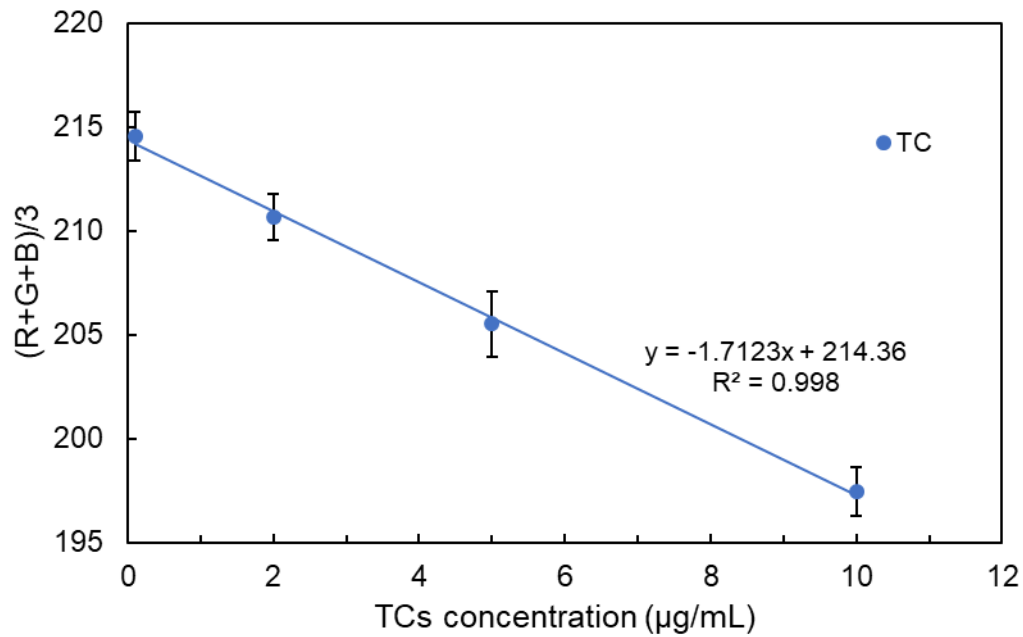
Figure 0.16- Normalized calibration line of TC.
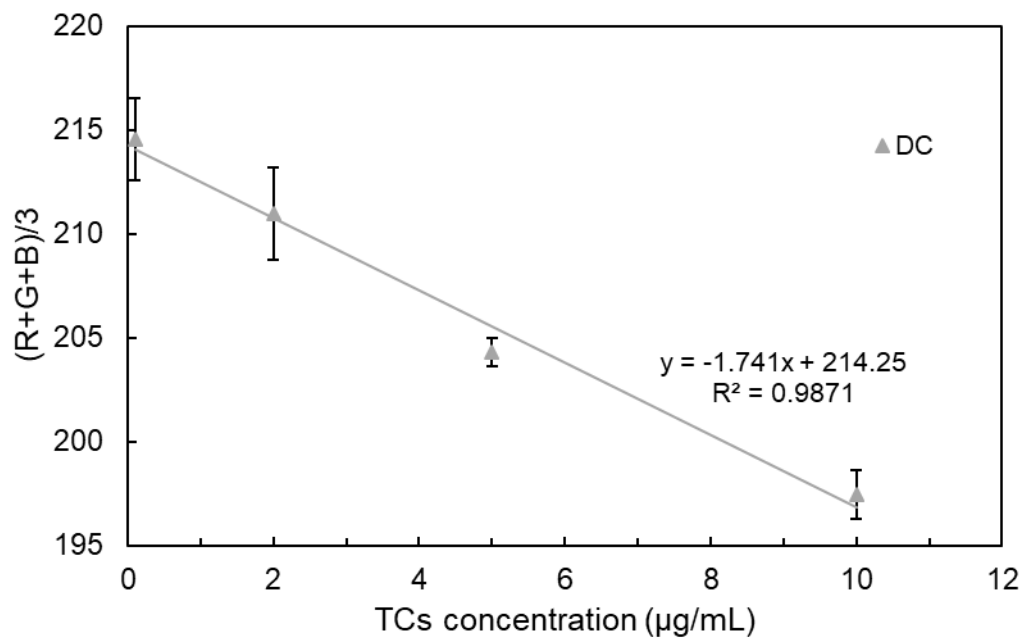
Figure 0.17- Normalized calibration line of DC.
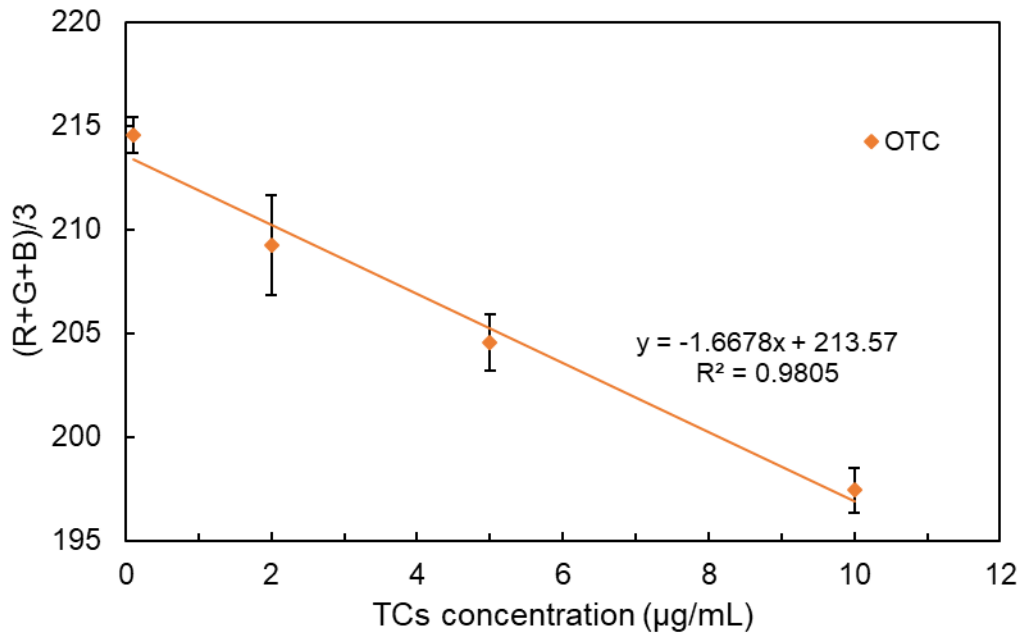
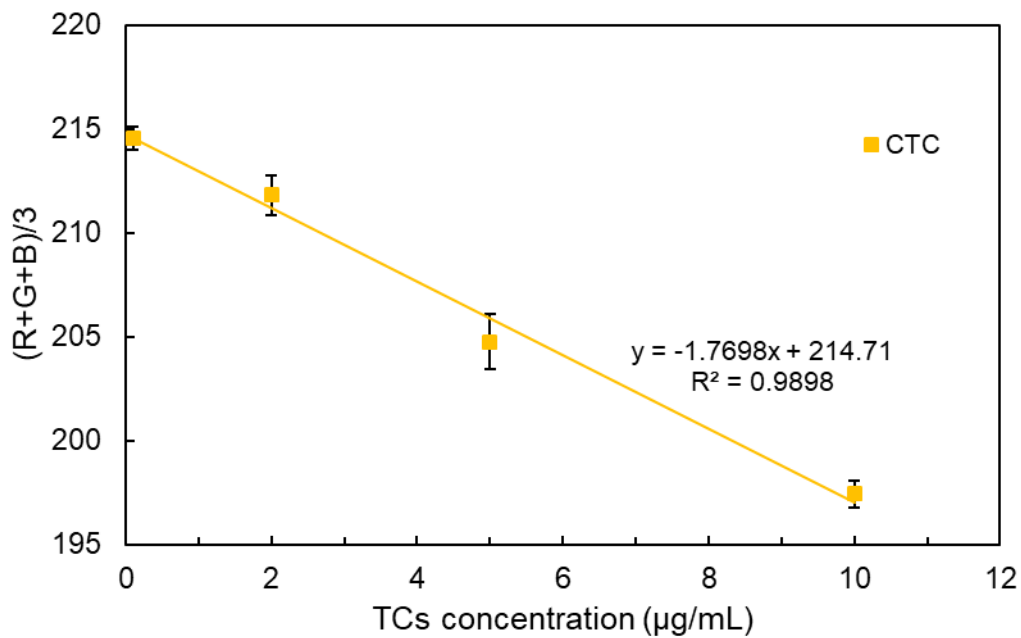**Figure 0.18**- Normalized calibration line of OTC.

Figure 0.19- Normalized calibration line of CTC.

H – Forms of milk sample treatment and solution results

Table 0.1- Forms of milk sample treatment and results.

Ways of milk sample treatment	Procedure	Results
Ø	TC solutions were diluted in milk with any treatment.	
I	McIlvane/ethylenediaminetetraacetic acid (EDTA) solution was prepared by adding 0.45 g of disodium hydrogen phosphate dihydrate, 0.11 g of EDTA and 0.39 g of citric acid monohydrate into 30 ml water. A 10 ml sample of milk spiked with standard TC, was mixed in a 50 ml plastic centrifuge tube with 30 ml of the McIlvane/EDTA solution. The solution was agitated for 1 min using a vortex. The sample solutions were then centrifuged until the protein precipitated. The precipitate was disposed of and the solution was used for the colorimetric test. [57]	
II	TC-spiked real sample solutions were prepared by adding TC in five times diluted milk samples. [58]	
III	TC-spiked real sample solutions were prepared by adding TC in ten times diluted milk samples.	
IV	4 mL milk sample spiked with TC was placed into a 15 mL centrifuge tube, and diluted with water to 10 mL, then 2 mL of citric acid and 2 mL chloroform were added and mixed under vortex for 1 min. The mixture was then sonicated at 20ºC for 15 min and centrifuged at 9,000 rpm for 10 min to separate the deposit. The supernatant was transferred into another centrifuge tube and centrifuged at 9,000 rpm for 10 min	

and the final solution was used for
detection. [59]

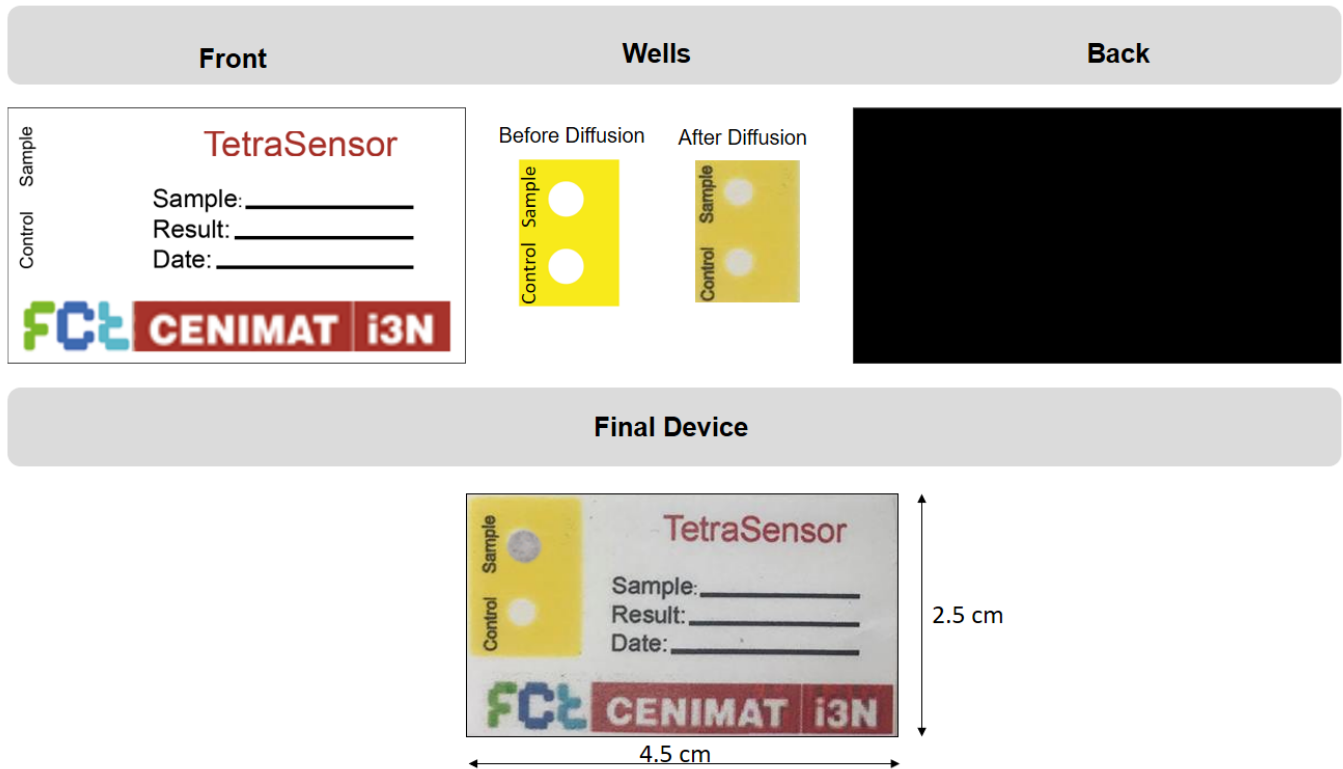## I – Prototype of the colorimetric paper-based biosensor

Figure 0.20- Prototype of the colorimetric paper-based biossensor.